Evolution of the flow structures in an elevated jet in crossflow

Cite as: Phys. Fluids **32**, 015102 (2020); https://doi.org/10.1063/1.5129498
Submitted: 29 September 2019 . Accepted: 13 December 2019 . Published Online: 02 January 2020

Sachidananda Behera, and Arun K. Saha

Physics of Fluids ARTICLE scitation.org/journal/phf

Evolution of the flow structures in an elevated jet in crossflow

Cite as: Phys. Fluids 32, 015102 (2020); doi: 10.1063/1.5129498
Submitted: 29 September 2019 • Accepted: 13 December 2019 •
Published Online: 2 January 2020

Sachidananda Behera and Arun K. Saha[a)]

AFFILIATIONS

Department of Mechanical Engineering, Indian Institute of Technology Kanpur, Kanpur 208016, India

[a)]Author to whom correspondence should be addressed: aksaha@iitk.ac.in

ABSTRACT

The characteristic flow features of an elevated square jet in crossflow (EJICF) are studied numerically using large eddy simulation. The effect of jet to crossflow velocity ratio, also called velocity ratio (VR), on the flow field of an elevated jet in crossflow (EJICF) is investigated. All the computations are carried out at a Reynolds number (Re) of 20 000, based on the outer width of the stack (d) and free stream crossflow velocity (U_∞), for four different velocity ratios (VR), namely, 0.5, 1.0, 1.5 and 2.0. The stack used in this study has an aspect ratio $h/d = 7$. The shear-improved Smagorinsky model has been used to account for the subgrid scale stress while solving the filtered three-dimensional unsteady Navier-Stokes equations. The modes of shedding in the stack wake are analyzed using both instantaneous and phase-averaged data. It is found that at a low jet to crossflow velocity ratio ($VR = 0.5$), the stack wake exhibits two different modes of shedding, symmetric and antisymmetric, similar to the wake of a wall mounted finite-size cylinder. At higher velocity ratios ($VR \geq 1$), the stack wake shows the presence of only antisymmetric modes of shedding. It is also found that velocity ratio (VR) has a profound effect on the source of vorticity of the jet shear layer structures near the upwind side. At $VR = 0.5$, the upstream sides of the jet shear layer structures are found to draw their vortices from the outer surface of the stack boundary layer. At higher VR, they seem to be fed by the vorticity of the boundary layer developed on the inner wall surface of the stack. Both jet vortices and stack wake vortices are found to be present in the jet wake, and the shedding frequency of both the jet wake and the stack wake is found to be same. The spatial evolution of the counter-rotating vortex pair in the case of an EJICF is found to be similar to that of a JICF.

I. INTRODUCTION

The complex flow configuration of a jet issuing into a crossflow has been widely studied in the past owing to its wide range of industrial and engineering applications. Depending on the source from which the jet is issued into the crossflow, it is categorized either as a jet in crossflow (JICF) or an elevated jet in crossflow (EJICF). In the case of a JICF, the jet is issued from an orifice on a wall and is associated with applications such as turbine blade cooling, fuel injectors, V/STOL aircrafts, and dilution holes in combustors. For an EJICF, the jet is issued from an elevated source in the form of a stack mounted on a wall and has a wide range of environmental applications such as chimneys, stack flares, cooling towers, and discharge of effluents into rivers or lakes. The JICF is characterized by a complex three-dimensional flow field owing to the interaction between the jet, jet wake, and the wall boundary layer. The complexity of the flow field in the case of EJICF increases further due to the presence of the stack and the interaction between the jet, jet wake, stack wake, and the wall boundary layer. The flow field of the JICF is studied in detail in the open literature, but the literature on the EJICF is limited as most investigations focused more on the JICF.

As highlighted earlier, the JICF has been studied extensively in the past with significant focus on the jet trajectories,[1–5] entrainment and mixing,[3,4,6–8] turbulent statistics,[2,9–14] turbulent crossflow conditions,[15–17] and flow structures. The dominant and distinctive vortical structures associated with the JICF are jet shear layer vortices, the horseshoe vortex system, the wake vortices, and the counter-rotating vortex pair (CRVP). The formation mechanism of the jet shear layer vortices has been investigated by many researchers in the past.[6,10,11,18–25] Kelso *et al.*[21] suggested that the jet shear layer rolls up near the upstream side of the jet like Kelvin-Helmholtz instability, which is found to move close to the jet exit with increasing Reynolds number. At very low Reynolds numbers (typically below 100) and low velocity ratios (ratio of the jet to crossflow velocity), a different

mechanism was proposed by Blanchard *et al.*[23] for the formation of the jet shear layer vortices. They suggested that instead of the Kelvin-Helmholtz type of instability, the formation of the jet shear layer vortices can be explained by the "Landman and Saffman" theory.[26] The leading edge jet shear layer vortices are found to be more regular in nature compared to the trailing edge jet shear layer vortices. These shear layer structures are found to be strongly dependent on parameters such as Reynolds number, velocity ratios, and even the ratio of the boundary layer thickness to the jet diameter.[18,21,25] The horseshoe vortex system in the case of JICF has also been studied extensively by many authors in the past.[20,21,27–29] The horseshoe vortex system depends mainly on the Reynolds number (Ref. 29), and multiple structures are observed with an increase in the Reynolds number. As the boundary layer becomes turbulent with increasing Reynolds number, the horseshoe vortex system becomes recognizable only in the time-mean flow. Kelso and Smits[28] showed that the horseshoe vortex system in the JICF are strongly dependent on the velocity ratio and can become steady, oscillating, or coalescing depending on the velocity ratio. The CRVP structure, which is a dominant flow feature for both the JICF and EJICF, forms due to the interaction between the jet and crossflow. The CRVP initiates in the jet near field and becomes a dominant flow feature in the far field. The formation mechanism of the CRVP has motivated a lot of works in the past, which include the work of Coelho and Hunt,[30] Kelso *et al.*,[21] Moussa *et al.*,[6] Sykes *et al.*,[31] Yuan *et al.*[25] Moussa *et al.*,[6] and Coelho and Hunt[30] suggested that the CRVP is formed from the shear layer emanating from the jet pipe exit, which rolls up to create vortex rings that are swept by the crossflow at different rates, thus deforming and bundling them into the CRVP. It is also suggested that the CRVP has mainly a mean-flow structure although it may have an unsteady component.

The wake vortices of a JICF have drawn a lot of attention from researchers around the globe.[6,20,21,32,33] However, the mechanism and source of the wake vortices has been a point of debate for long time. Earlier to understand the jet wake structures of the JICF, analogies are drawn with the wake behind solid cylinders, and it is suggested that vortex shedding in the jet wake is similar to the flow past a solid obstacle.[32] McMahon *et al.*[32] also suggested that the Strouhal numbers for the flow past the circular cylinder and JICF are in qualitative agreement, provided that the width of the jet spreading some distance away from the jet exit is used as the length scale instead of the jet diameter. Fric and Roshko[20] through their flow visualization study showed that the origin and formation of the wake vortices in the case of a JICF is fundamentally different from that of the flow past solid obstacles. They observed that the flow around a transverse jet cannot separate from the jet and will not shed vortices into the wake. They also suggested that for constant density fluids (like they have considered where both jet and crossflow fluid have the same density), vorticity cannot be generated at the interface of the jet and crossflow fluid but must have their source at a solid surface. They showed that, in the case of JICF, the wake vortices have their origin in the boundary layer of the wall of the pipe from which the jet is issued. This theory has subsequently been confirmed by various other researchers.[3,21,34] However, some jet fluids have also been observed in the jet wake by various authors.[3,8,35]

In contrast to the JICF, the vortex system associated with the EJICF has been rarely studied in the literature. The mechanism of the formation of various flow structures in the case of EJICF is expected to be fundamentally different from that of the JICF, as the crossflow seems to interact with both the jet and the stack (from which the jet is issued into the crossflow). The wake behind the EJICF was investigated by Eiff *et al.*[36] using point measurements of velocity at multiple locations. Their spectral analysis revealed that the shedding behind the stack is very similar to that of a solid cylinder. They also suggested that the frequency related activity in the jet wake is directly linked to that of the stack wake and the frequency is always found to scale with the stack diameter. In contrast to Fric and Roshko,[20] who suggested that the jet cannot shed any of its vortices in the case of a JICF, Eiff *et al.*[36] through their temperature measurements showed that the jet does shed some of its vortices in the case of an EJICF. In an extension to their previous work,[36] Eiff and Keffer[37] used a pattern-recognition technique to characterize the flow throughout the wake up to the bent-over-jet region. They observed that the wake structures on one side of the symmetry plane are linked to the other structures on the opposite side of the plane in the jet region, and hence, these structures split before they are linked. They also reported that the jet wake structures contribute to the overall vorticity content of the CRVP.

Apart from the jet wake, the jet shear layer structures in the case of EJICF are also studied in the literature. Huang and Lan[38] experimentally studied the characteristic and evolution of the shear layer of an elevated round jet in crossflow. They came up with five characteristic flow features for the upwind side jet shear layer: "*mixing-layer type vortices*," "*backward-rolling vortices*," "*forward-rolling vortices*," "*swing-induced mushroom vortices*" and "*jet type vortices*" depending on the velocity ratio. They also reported that in the jet shear layer, the Strouhal number decreases exponentially with an increase in the jet-to-crosswind momentum ratio. Saïd *et al.*[39,40] investigated the flow structures near the tip region of the stack for an EJICF using particle image velocimetry (PIV). They suggested that the rotational direction of the Kelvin-Helmholtz induced shear layer vortices depends on the velocity ratio.

The effect of the velocity ratio on the flow structures of the EJICF has also been explored by many researchers previously. Huang and Hsieh[41] used a laser Doppler velocimeter to characterize the flow field of an EJICF for various velocity ratios. They defined four different flow regimes depending on the velocity ratios: "*downwash*," "*crosswind-dominated*," "*transitional*," and "*jet-dominated*." They also reported that large amount of jet fluids are pulled into the stack wake in the case of downwash dominated and crosswind-dominated flow due to the presence of a clockwise rotating vortical structure in the near wake of the EJICF. The same authors[42] in another study did a complete topological analysis of the flow field of an EJICF using critical point theory and showed that the flow topology in terms of critical points also changes with the change in the velocity ratio.

The effect of jet-to-crossflow velocity ratio (VR) was also studied by Adaramola *et al.*[43] for the turbulent wake of an elevated round jet in crossflow. The stack in their study was partially immersed in a turbulent boundary layer of thickness, $\delta/h = 0.5$, at the position of the stack. Similar to Huang and Hsieh,[41] they also reported three distinct flow regimes depending on the values of the velocity ratio (VR), which are "*downwash dominated*" ($VR < 0.7$), "*crosswind dominated*" ($0.7 \leqslant VR < 1.5$), and "*jet-dominated*" ($VR \geqslant 1.5$). They observed that at the midspan of the stack, the vortex formation length decreases with an increase in velocity ratio, suggesting

a two-dimensional wake similar to the wake of an infinite cylinder. They also showed that with the increase in velocity ratio, the Strouhal number of the stack approaches that of an infinite cylinder. In another study by the same authors,[44] the effect of velocity ratio on the streamwise vortex structures was analyzed. They found that in the case of downwash and crosswind dominated flow, only two pairs of counter-rotating streamwise vortices exist in the stack wake. One vortex pair was found near the tip region of the stack, and the other vortex pair was found close to the bottom wall. However, for the jet-dominated flow, they also found another vortex pair above the free-end of the stack with orientation the same as that of the base vortex. Arora and Saha[45] studied the effect of velocity ratio on the particle concentration in the case of an EJICF and linked them to the flow field dynamics. Their numerical study was restricted to a very low Reynolds number of $Re = 250$.

A detailed and careful study of the literature implied that most of the previous investigations on the EJICF focused on the jet wake or the jet shear layers or the mean flow field characteristics, with a little attention on the modes of shedding in the stack wake. The present study is the very first attempt where the modes of shedding associated with the stack wake of an EJICF is analyzed for different velocity ratios. Apart from that, the source of vortices in the case of the jet shear layer structures is expected to be different from that of the case of JICF, at least under different conditions of velocity ratios due to the presence of the stack. Therefore, the source of jet shear layer vortices under different conditions of velocity ratios is also investigated in this study. The open literature suggests that in the case of JICF, the boundary layer on the wall of the pipe from which the jet is issued is the source of vorticity for the vortices in the jet wake,[20] i.e., the jet cannot shed any of its vortices. However, for the EJICF, the study of Eiff *et al.*[36] suggests that the jet can shed its vortices and the jet wake vortices have their origin in the inner-wall boundary layer of the stack opposed to the outer wall. Since the findings of Fric and Roshko[20] and Eiff *et al.*[36] contradict each other, the present study further looks into the source of vortices in the jet wake of the EJICF. It is also worth mentioning that almost all the previous studies on the EJICF are experimental in nature, with Arora and Saha[45] being the exception who performed a direct numerical study (DNS) at a low Reynolds number ($Re = 250$).

In general, the Reynolds number encountered in the case of residential chimneys is one order less than those of industrial chimneys or cooling towers, which are of the order of 10^5. In both cases, the associated flow fields are turbulent in nature. In the present study, the Reynolds number was kept of the order of 10^4 so that the flow field becomes turbulent as the crossflow interacts with the jet and stack, respectively. The literature reveals that for a wall mounted square cylinder with $AR > 3$, the flow from the free-end of the cylinder does not reach the bottom wall, and with an increase in AR, the interaction between the bottom wall and flow from the free-end of the cylinder is minimized. Therefore, the aspect ratio of the square stack is kept at 7 with a stack thickness of 0.02 in the present study to avoid the effect of the bottom wall on the flow near the tip region of the stack. The stack thickness is kept as minimum as possible to avoid any effect of it on the jet shear layer structures. The present large eddy simulation (LES) study has been carried out at a Reynolds number (Re) of 20 000, where Re is based on the outer width of the square-stack (d) and the free-stream velocity (U_∞). The displacement thickness of the bottom wall boundary layer at the stack position (in the absence of the stack) is found to be quite low because of the fact that the incoming velocity profile is taken to be uniform. In case of application of pollutant dispersion from a chimney, the wind speed of the crossflow may vary throughout the day, while the jet velocity is dictated by the thermal draft present in the chimney. Therefore, the variation in the two velocities alters the velocity ratio (jet to crossflow velocity ratio, VR). In any particular day, the velocity ratio of a chimney varies widely as the crossflow and the thermal field in the chimney change continuously. To mimic this situation, four different velocity ratios (VR), namely, $VR = 0.5$, 1.0, 1.5 and 2.0, are considered in the present study. The details of both near and far-field flow characteristics are reported with the help of instantaneous, time-averaged flow field and corresponding turbulent statistics. To the best of authors' knowledge, this is the very first study where a large eddy simulation (LES) is performed to analyze the characteristic flow features of an EJICF. The present study also brings out some of the essential and important flow features associated with EJICF flows relating downwash and upwash phenomena.

II. NUMERICAL METHODOLOGY

The flows at high Reynolds numbers have a wide range of temporal and spatial scales. The computation of such a flow requires an accurate numerical methodology to resolve these scales. With an increase in the Reynolds number, the size of the smallest of these scales decreases and hence defines the grid resolution to be used. The LES turbulence model has emerged as a popular alternative to the DNS study for high Reynolds number turbulent flows, as the computational cost associated with the DNS of turbulent flow is extremely high. The governing equations for the LES are obtained by applying a spatial filtering operation to the Navier-Stokes equations so that the smallest and largest scales are clearly separated. The spatial filtering operation has been carried out by decomposition of the flow field variables as $u_i = \widetilde{U}_i + u_i'$, where $\widetilde{U}_i$ indicates the filtered/resolved flow variable and u_i' refers to the subgrid scale (SGS) motion. In the LES approach, $\widetilde{U}_i$ is directly computed on the grid while the effect of u_i' on the large scale is suitably modeled.

The filtered governing equation for the LES is obtained after using the aforementioned decomposition technique and then applying spatial filtering operation on the Navier-Stokes equations.[46] The resulting governing equations can be given as follows:

$$\frac{\partial \widetilde{U}_i}{\partial x_i} = 0, \tag{1}$$

$$\frac{\partial \widetilde{U}_i}{\partial t} + \widetilde{U}_j \frac{\partial \widetilde{U}_i}{\partial x_j} = -\frac{\partial \widetilde{p}}{\partial x_i} + \frac{1}{\mathrm{Re}} \frac{\partial^2 \widetilde{U}_i}{\partial x_j^2} - \frac{\partial \tau_{ij}}{\partial x_j}, \tag{2}$$

where $\tau_{ij} = \widetilde{u_i' u_j'} - \widetilde{U}_i \widetilde{U}_j$ is the SGS stress tensor. The SGS stress tensor is computed using a "Shear-Improved Smagorinsky" model, where the anisotropic part of the SGS term is given as

$$\tau_{ij} = \frac{1}{3}\delta_{ij}\tau_{kk} - 2\nu_T \widetilde{S}_{ij}. \tag{3}$$

The eddy viscosity ν_T is given by

$$\nu_T = (C_s \Delta)^2 (|\widetilde{S}| - |\langle \widetilde{S} \rangle|), \tag{4}$$

TABLE I. Comparison of integral parameters with the LES data of Srinivas *et al.*[50] and Sohankar *et al.*[51] and the experimental data of Lyn *et al.*[52]

Source	$Re \times 10^4$	$\overline{C_d}$	$\overline{C_l}$	C_d^{rms}	C_l^{rms}	Strouhal-number (St)
Present simulation	2.14	2.17	0.0	0.23	1.17	0.131
Lyn *et al.*	2.14	2.10	...	...	...	0.132
Srinivas *et al.*	2.14	2.14	0.0	0.17	1.12	0.135
Sohankar *et al.*	2.20	2.25	...	0.20	1.50	0.130

where C_s is the standard Smagorinsky constant and Δ denotes the grid spacing, which is given as $\{(\Delta x)(\Delta y)(\Delta z)\}^{\frac{1}{3}}$. More details about the "Shear-Improved Smagorinsky" model can be found in Refs. 47 and 48.

In Eqs. (1) and (2), all length and velocity scales are nondimensionalized by using the outer width of the stack, d, and free-stream velocity, U_∞, respectively. Similarly, the time and pressure are nondimensionalized by d/U_∞ and ρU_∞^2, respectively. The numerical technique followed in the present investigation is an improved version of the Marker and Cell (MAC) algorithm of Harlow and Welch.[49] A second order Adams-Bashforth scheme is used for the temporal discretization of the convective terms, whereas the diffusion terms used the Crank-Nicolson scheme. The pressure Poisson equation is solved using a Gauss-Seidel method with an under relaxation factor to achieve the desired convergence of the pressure correction process. The equations are discretized on a staggered nonuniform grid such that the velocities are defined at the cell face to which they are normal and pressure is defined at the center of the cells. The convective terms are discretized using weighted average second order central difference and third order upwind-biased schemes, and the diffusion terms are discretized using a second order central difference scheme. The simulations are carried out using a finite-difference based in-house code with the Message Passing Interface (MPI) frame work. The details of the code implementation could be found in Ref. 48.

In the literature, no experimental as well as numerical work is available for a jet ejecting from a square shape stack and only few experimental studies are available with the jet ejecting from a circular stack. Since the actual code used here is developed for the Cartesian coordinate system, simulating a circular stack will require special techniques such as the immersed boundary method. Implementing the immersed boundary method would not only have added more complexities but also have made the computations a lot more expensive. Therefore, for code validation, two different sets of problems are chosen: (i) a spatially developing circular free jet at Re = 10 000 and (ii) flow past an infinite size square cylinder at Re = 21 400. In the case of the circular free jet, the jet half-width, radial variation of the time-mean streamwise velocity at various streamwise locations, radial variation of the Reynolds stress components, and radial variation of the components of the triple moment tensor are compared with the existing literature. The details of these comparisons can be found in one of the authors' previous work.[48] For the flow past the square cylinder, the code validation is performed against the numerical results of Srinivas *et al.*[50] and Sohankar *et al.*[51] and experimental results of Lyn *et al.*[52] The computational domain and the boundary conditions, for simulating the flow past the square cylinder, are chosen to be the same as those of Srinivas *et al.*[50] Table I compares the various integral parameters, such as overall (time- and span-averaged) drag and lift coefficients, rms quantities of lift and drag coefficients, and Strouhal number, with those of Srinivas *et al.*,[50] Sohankar *et al.*,[51] and Lyn *et al.*[52] The drag and lift coefficients and their rms values are all corrected for the blockage according to the Maskell scheme.[53] A good match between the present results and the data in the literature has been observed. The comparison of time-averaged streamwise velocity recovery along the wake centerline is shown in Fig. 1(a). The present study shows a good comparison for the time-averaged streamwise velocity recovery along the streamwise direction with the

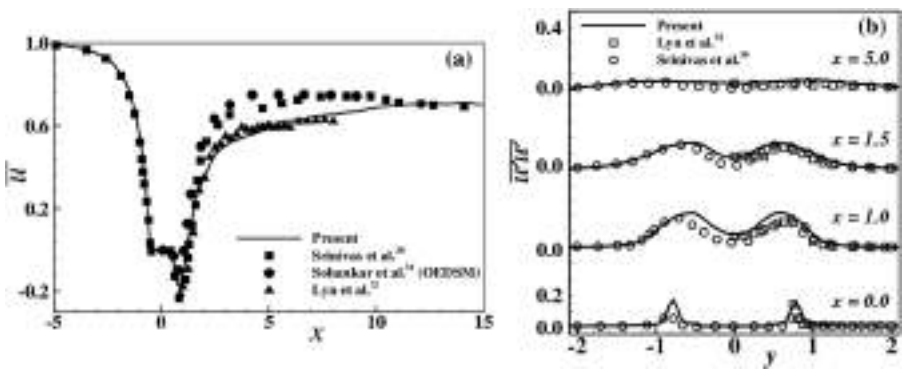

FIG. 1. (a) Time-averaged streamwise velocity recovery along the wake centerline. (b) Time-averaged streamwise normal stress distribution at x = 0.0, 1.0, 1.5, and 5.0.

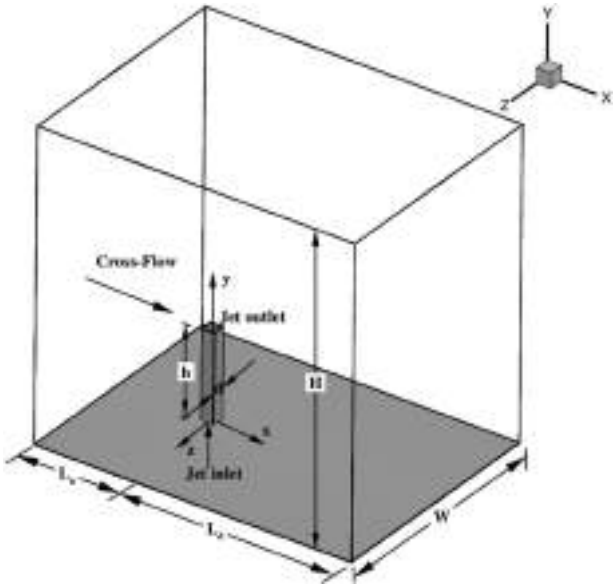

FIG. 2. Three-dimensional computational domain (all the dimensions are scaled with the stack outer width *d*).

experimental results of Lyn *et al.*[46] Figure 1(b) shows the distribution of normal streamwise stress at various streamwise locations. A good match between the present data and those of Lyn *et al.*[52] and Srinivas *et al.*[50] has been observed. Additional validation of the code for the present geometry has also been undertaken while discussing the results for the present geometry.

The computational domain is shown in Fig. 2, and the dimensions related to the computational domain are $W = 18d$, $H = 24d$, $L_u = 7.5d$, and $L_d = 18d$. The domain extents are so chosen that the flow field is free from any effect of locations of boundaries. The aspect ratio of the stack is taken as $h/d = 7$. The boundary conditions used in the present numerical simulation are given as follows:

1. A constant uniform streamwise velocity (U_∞) of unity is prescribed at the crossflow inlet, along with $v = w = 0$.
2. At the outflow boundary of the computational domain, a convective outflow boundary condition given by Eq. (5), proposed by Orlanski,[54] has been used,

$$\frac{\partial u_i}{\partial t} + u_c \frac{\partial u_i}{\partial x} = 0. \tag{5}$$

   Here, u_i corresponds to the three velocity components and u_c is the convective velocity at the outflow boundary plane.
3. The bottom surfaces of the computational domain is modeled as a no-slip and impermeable wall, except for the region enclosed by the stack.
4. At the bottom of the stack (zone from which the jet is issued), a constant uniform vertical velocity (v) depending on the velocity ratio is used with other two components of velocity to be zero ($u = w = 0$).
5. Both the inner and outer surfaces of the stack are modeled as a no-slip and impermeable wall.
6. The rest of the confining surfaces, i.e., top, and the two transverse boundary surfaces are modeled as free-slip boundaries.

Nonuniform orthogonal grids with clustering of grid points near the bottom-wall as well as near all the solid walls of the stack and stack exit have been used in the present computation. The minimum grid size near the bottom wall, stack surfaces, and stack exit is kept at 0.004. The cells are then stretched away in a proper manner such that a reasonable balance between accuracy and computational effort could be maintained. It is essential to show that the computational results revealing the dynamics of EJICF are independent of the grid size. Therefore, a grid sensitivity test is carried out using three different grid sizes, namely, 218 × 192 × 174 (coarse), 266 × 237 × 206 (intermediate), and 314 × 282 × 242 (fine), for the computational domain shown in Fig. 2. The near wall spacing for the three different grid sizes, i.e., coarse, intermediate, and fine, is chosen to be 0.01, 0.004, and 0.0025, respectively. The details of the grid sensitivity test are shown through the time-averaged streamwise velocity recovery along the centerline on the plane $y/d = 6.3$ and the spanwise variation of the time-mean shear stress component ($\overline{u'v'}$) at the axial location, $x/d = 5.0$, on the symmetry plane ($z/d = 0$) [Figs. 3(a) and 3(b)] for the three grid sizes. The predictions by the intermediate and finest grid are found to have a close match. Therefore, the results obtained by using the grid 266 × 237 × 206 are considered to

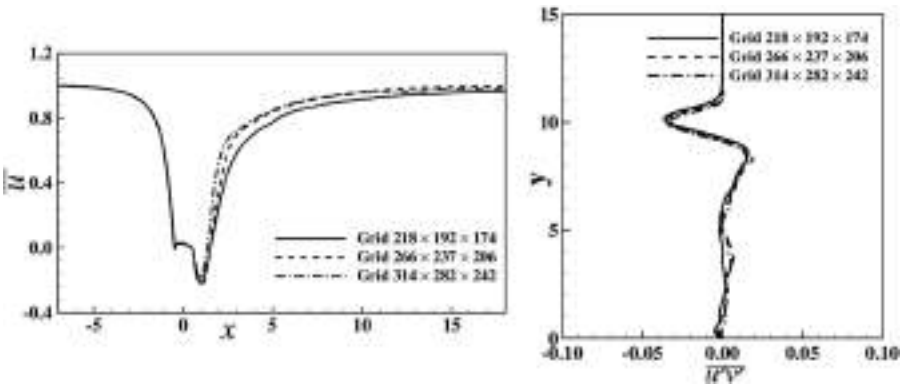

FIG. 3. Grid independence test: (a) variation of the time-averaged streamwise velocity along the centerline on the plane $y/d = 6.3$ and (b) spanwise variation of the time-mean shear stress component ($\overline{u'v'}$) at an axial location, $x/d = 5.0$, on the symmetry plane $z/d = 0$.

be grid-independent and hence used for all the simulations carried out in the present study.

III. RESULTS AND DISCUSSION

In this section, the results of LES are analyzed to provide an insight into the effect of velocity ratio on the flow field dynamics of EJICF. The investigation includes the effect of velocity ratio on the modes of shedding of stack wake, jet shear layer structures, jet wake structures (analyzed from instantaneous data), time-averaged flow field, and turbulent fluctuating fields. However, before that the associated flow structures in the case of EJICF are discussed in brief.

The instantaneous isocontour of λ_2 is plotted in Fig. 4 showing the highly complex vortex flow pattern in the case of an EJICF at velocity ratio $VR = 2$. The vortex flow pattern reveals the presence of multiple horseshoe vortex structures in-front of the stack formed due to the separation of the boundary layer in-front of the stack. The bottom-wall vortices are also observed in the wake region of the stack. In the wake region of the stack, the shedding structures from one side of the stack are found to be connected to those on the opposite side through the riblike structures. Both the stack wake and the jet wake structures show the presence of hairpin type of structures. On the sidewall of the stack, the separating shear layers seem to undergo a Kelvin-Helmholtz type instability creating stack shear-layer vortices that seem to extend over the full span of the stack. The jet issuing from the stack interacts with the crossflow, leading to the formation of jet shear-layer vortices. The source of vorticity in the case of jet shear-layer structures and their dependency on the velocity ratio (VR) are also discussed in Sec. III B.

A. Stack wake

In this section, the mode of shedding along the stack height of an EJICF is analyzed using both the instantaneous and phase averaged spanwise vorticity (ω_y) fields. It is observed that the mode of shedding in the stack wake of the EJICF is dependent on the jet to crossflow velocity ratio (VR). Similar to the wake of a wall mounted finite-length square cylinder,[55–58] the stack wake of an EJICF shows two different modes of shedding, namely, symmetric and antisymmetric modes. The antisymmetric mode of shedding is found to be the dominant mode of shedding in the stack wake with the symmetric mode of shedding occurring intermittently in-between. Similar observations for the wake of a wall mounted finite-size square cylinder were reported earlier by Wang and Zhou[57] (for a high Reynolds number, $Re = 9300$) and Behera and Saha[58] (for a low Reynolds number, $Re = 250$). As suggested earlier, the mode of shedding in the stack wake of the EJICF is closely related to the velocity ratio (VR), where the symmetric mode of shedding is found to occur only at a low velocity ratio, $VR = 0.5$. At higher velocity ratios, $VR \geq 1.0$, only antisymmetric mode of shedding is observed in the stack wake with no evidence of symmetric mode of shedding. To analyze the symmetric and antisymmetric shedding behavior of the stack wake at $VR = 0.5$, the instantaneous spanwise vorticity field on the horizontal plane, $y/d = 5.6$, is plotted in Fig. 5.

From Fig. 5, it is observed that the near wake of the stack on the plane $y/d = 5.6$ shows the presence of both symmetric and antisymmetric modes of shedding at two different instances of time. However, away from the near wake, the antisymmetric mode of shedding is observed to be dominant at all time instances. It is also found that the symmetric and antisymmetric mode of shedding is more of a phenomenon associated with the upper half of the stack wake compared to the lower half. It is found that the stack wake up to a vertical height of $y/d = 4.2$ from the bottom wall shows only the presence of antisymmetric modes of shedding, while beyond it, both symmetric and antisymmetric modes of shedding were observed at $VR = 0.5$. The absence of symmetric modes of shedding up to the vertical height of $y/d = 4.2$, at low velocity ratio $VR = 0.5$, may be largely due to the weak downwash experienced by the stack wake up to the same vertical height, i.e., $y/d = 4.2$, while the strength of downwash is expected to be stronger in the remaining vertical length of the stack height. Similar arguments for the occurrence of symmetric modes of shedding, in the case of a wall mounted finite-size cylinder wake, was given by Behera and Saha.[58] They showed

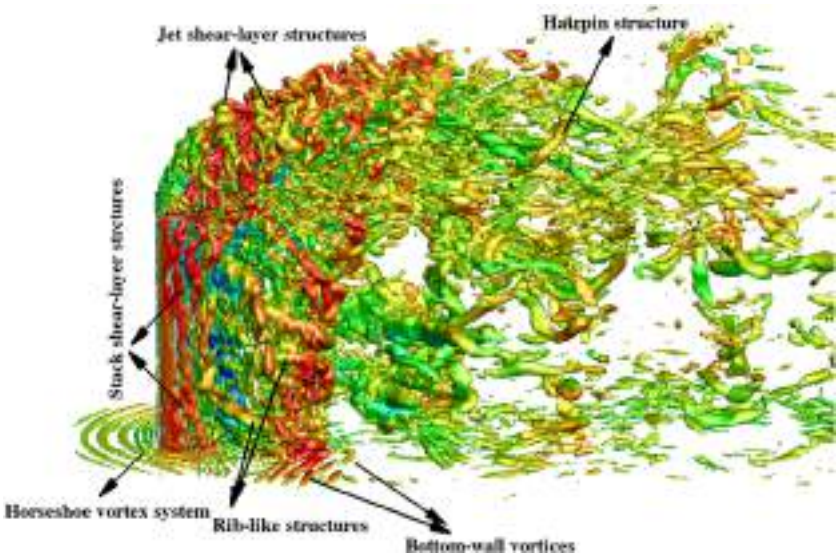

FIG. 4. Isocontour of λ_2 colored with the streamwise velocity at the velocity ratio, $VR = 2$.

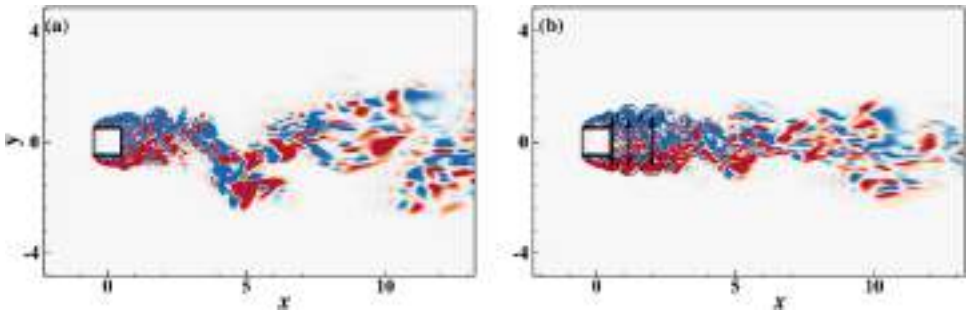

FIG. 5. Instantaneous contour of the spanwise vorticity (ω_y) on the horizontal plane, y/d = 5.6, at velocity ratio VR = 0.5: (a) antisymmetric mode of shedding and (b) symmetric mode of shedding.

that for a finite-size square cylinder of aspect ratio AR = 7, the symmetric mode of shedding is strongly dependent on the strength of downwash or upwash flow experienced by the flow from the cylinder free-end or bottom-wall, respectively. They also revealed that as the wake experiences the maximum downwash/upwash flow, symmetric mode of shedding occurs; otherwise, the antisymmetric mode of shedding persists. With the increase in the velocity ratio in the case of EJICF, the downwash effect gradually decreases as the jet pushes deeper into the crossflow and thereby increases the effective height of the stack. Consequently, this higher effective stack length suppresses the strength of the downwash flow from the top of the stack. Figure 6 presents the variation of the strength of the downwash flow with increasing velocity ratio.

Figure 6 shows the phase-averaged isosurfaces of the negative vertical velocity, representing the downwash flow for all the four cases considered in the present study. Clearly, Fig. 6 illustrates that as the velocity ratio increases, the strength of the downwash flow decreases. Thus, at $VR \geq 1.0$, only an antisymmetric mode shedding was observed along the height of the stack. Although the presence of both symmetric and antisymmetric modes of shedding behind a wall-mounted finite-size cylinder was reported earlier, but a similar phenomenon for the stack wake of an EJICF at low VR was never reported earlier. Huang and Lan,[38] Said *et al.*,[40] and Arora and Saha[45] discussed about the presence of antisymmetric mode of shedding in the stack wake of an EJICF for $VR < 1.0$ but never showed or discussed about the presence of symmetric mode of shedding. To the best of our knowledge, it is the very first instance where the presence of both antisymmetric and symmetric modes of shedding is reported for the stack wake of an EJICF. We believe that as the velocity ratio is increased gradually, the stack wake shows the characteristics of the wake of an infinite cylinder. However, as the velocity ratio is decreased, the stack wake becomes more similar to the wake behind a wall-mounted finite-size cylinder. A wall mounted finite-length cylinder could be approximated as a special case of an EJICF, with VR = 0, where the downwash experienced by the stack wake is maximum and its strength gradually decreases with an increase in VR.

It should also be noted that the occurrence of symmetric and antisymmetric modes of shedding is also going to affect the loading or force acting on the stack, which could be very essential from the point of the structural design of stack. In the present study at a low velocity ratio, i.e., VR = 0.5, when both symmetric and antisymmetric shedding are observed in the stack wake, the drag and lift force acting on the stack are found to be different. The temporal variation of the lift force acting on the stack for VR = 0.5 is shown in Fig. 7 where it reveals periods of high amplitudes of

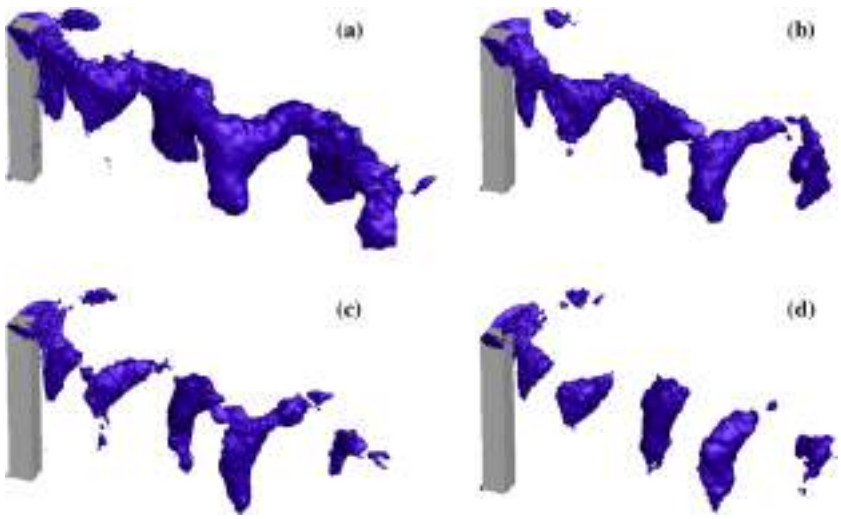

FIG. 6. Isosurface of the phase-averaged negative vertical velocity (v = −0.2) for various velocity ratios: (a) VR = 0.5, (b) VR = 1.0, (c) VR = 1.5, and (d) VR = 2.0.

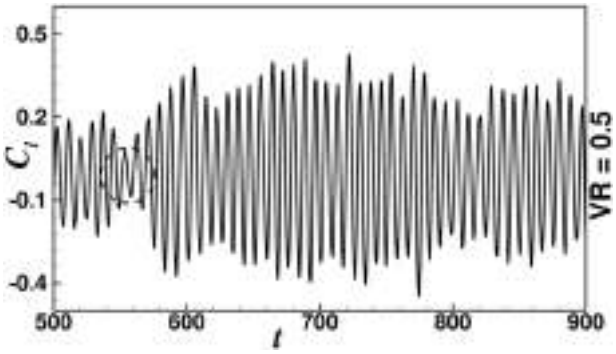

FIG. 7. Time-history of lift force (C_l) acting on the stack outer surface at velocity ratio VR = 0.5. The circled zone represents periods with lower amplitudes of C_l.

C_l along with instances of lower amplitudes occurring in-between. The duration and frequency of occurrence of lower amplitudes are found to be small compared to the higher amplitudes, and it is during these periods of low amplitude, symmetric mode of shedding occurs in the near wake of the flow; otherwise, antisymmetric mode of shedding prevails. The symmetric mode of shedding occurs intermittently for a short duration of time, and the repetition rate (or number of appearance) is quite small in comparison to the asymmetric mode of shedding, and hence, it does not have a fixed time interval associated with it. Similar to the lift force, the drag force is also found to be lower during the occurrence of symmetric modes of shedding compared to that during the antisymmetric modes of shedding.

B. Jet shear layer structure

An important flow feature of an EJICF is the jet shear layer structures. It is believed that for an EJICF, the shear layer coming out of the stack or the pipe undergoes Kelvin-Helmholtz type instability and separates from the edge of the stack, giving rise to the jet shear layer vortices.[40] It is also reported that the shear layer coming out of the stack rolls up at both the upwind and lee side of the stack, leading to the jet shear layer vortices, and the vorticity associated with these rolling is of the same sign as that of the stack inner wall shear layer vorticity.[21,25,40,59] For a JICF, irrespective of the jet to crossflow velocity ratio (VR), the jet shear layer vortices seem to draw its vorticity from the inner wall shear layer of the stack. However, for an EJICF, these findings are not necessarily true at all the jet to crossflow velocity ratios. The present sets of simulations for an EJICF for four different conditions of velocity ratios, i.e., VR = 0.5, 1.0, 1.5, and 2.0, highlight this aspect of the flow phenomenon, which was never reported earlier. Figure 8 shows the instantaneous jet shear layer of the EJICF for four different velocity ratios considered in the present study. The instantaneous shear layer plots shown in Fig. 8, for the four different values of VR, belong to the same phase of the instantaneous data. For VR = 0.5 [Fig. 8(a)], one can clearly observe that the upwind side of the jet shear layer is constantly fed with vortices developing on the front outer surface of the square cylinder or stack. However, as the velocity ratio is increased from VR = 0.5 to 2.0, the boundary layer vorticity coming out of the stack, formed on the inner walls of the stack, then becomes a dominant source of vorticity for the upwind side jet shear layer vortices. However, on the lee side, the jet shear layer always seem to have its vortices drawn from the boundary layer or shear layer formed at the internal walls of the stack. At VR = 0.5, one can observe that the incoming flow

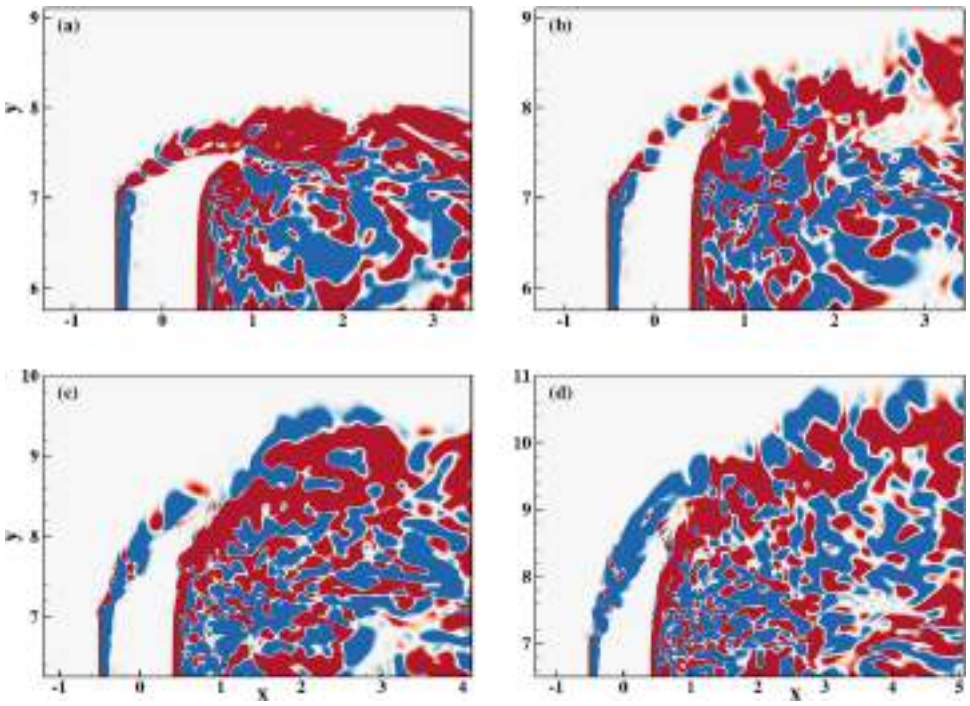

FIG. 8. Instantaneous contour of transverse-vorticity (ω_z) component showing the jet shear layer vortices on the symmetry plane z/d = 0 for various velocity ratios: (a) VR = 0.5, (b) VR = 1.0, (c) VR = 1.5, and (d) VR = 2.0.

separates at the front edge of the cylinder and rolls up to form the jet shear layer vortices having close resemblance to that of free-jet wake vortices on the upwind side of the jet. Although the jet shear layer on the upwind side mostly draws its vortices from the outer front surface of the stack, still weak secondary flow vortices having their origin in the boundary layer of the stack inner wall can also be seen [Fig. 8(a)]. It is observed that, near the upwind side, a positive vorticity field is associated with the shear layer of the front outer surface of the stack, while a negative vorticity field is associated with the boundary layer developed on the inner surface of the stack. At $VR = 0.5$, the jet fluid does not have enough momentum to sustain the impact of the high momentum crossflow. Hence, the stack inner-wall boundary layer coming out of the stack is pushed back into the stack itself, near the upwind side of the stack. As a result, at $VR = 0.5$, a positive vorticity field is found to be dominant at the upwind side of the jet shear layer. However, at higher VR, the inner stack boundary/shear layer coming out of the stack has enough momentum to sustain the impact of the crossflow, and hence, a negative vorticity field associated with the upwind side of the jet shear layer is found to dominant at higher velocity ratios. A small recirculation bubble is also observed closer to the stack exit for $VR = 0.5$, near the upwind side of the stack, and is found to be unsteady in nature. This recirculation bubble is shown and discussed later in the time-averaged flow field for $VR = 0.5$ in Sec. III D. However, at a higher velocity ratio, i.e., $VR = 1$, this recirculation bubble was only observed in the instantaneous flow, whereas it almost became flat and appeared very close to the inner front surface of the stack in the time-averaged flow field. At $VR > 1.0$, this recirculation vortex disappears completely in both instantaneous and time-averaged flow fields. This is probably due to the higher momentum of the jet that could resist the impact of crossflow and penetrates deeper into it, thereby avoiding the creation of the recirculation zone near the exit of the jet. In contrast to $VR = 0.5$, the upwind side of the jet shear layer at $VR = 1.0$ seems to draw its vortices from the shear layer developed on both the inner and outer front surfaces of the stack, and hence, a little away from the jet exit, one can clearly observe the alternate positioning of the inner and outer stack shear layer vortices. At $VR = 1$, both the jet and crossflow fluid have a similar momentum; as a result, the crossflow is not strong enough to suppress the upwind side shear layer coming out of the inner surface of the stack. Although a recirculation zone is created near the stack exit under the influence of crossflow, but it is not strong enough to completely suppress the stack shear layer coming out of the stack exit. As a result, both the shear layers, outer and inner, roll up near the upwind side of the stack and contribute to the jet shear layer vortices at the upwind side of the stack. At higher velocity ratios, i.e., $VR > 1$, it is observed that the stack shear layer coming out of the stack rolls up near both the ends of the stack (upwind and lee side) and form the jet shear layer vortices similar to the JICF. At higher velocity ratios ($VR > 1$), the high momentum shear layer coming out of the stack penetrates deeper in to the crossflow and pushes the leading edge shear layer upstream and then rolls up to form the upwind side jet shear layer vortices. However, for all the cases of VR, it is observed that the lee side of the jet shear layer always draws its vortices from the boundary layer developed within the lee side of the stack inner wall. It is also found that the vortices in the upstream side of the jet shear layer are more regular in comparison to the downstream shear layer, where the rolling up of the shear layer is quite irregular. The vertical distance away from the stack, where the vortices from both the upwind and downwind sides of the jet shear layer interacts are seen to be dependent on the VR as it is found to increase with increasing VR. However, the axial or streamwise location where the vortices from both upwind and downwind sides of the jet shear layer interact is found to oscillate. For $VR = 1.5$ and 2.0, vortices from the upwind and downwind shear layers interact in a manner such that a gap in the jet flow of the order of stack width is observed (see Fig. 9). Similar observations were also reported in Ref. 25 in their LES study for a JICF at $VR = 2.0$ and 3.3. As suggested in Ref. 25, this gap on the upstream side of the jet shear layer is important for entrainment of the crossflow fluid by the jet.

C. Jet wake

The jet wake structures of an EJICF is found to be more complex in nature in comparison to the stack wake. To analyze the jet wake structures, a phase-averaging technique is used, where periodicity associated with the stack wake is used to define the phases. To ensure that the number of shedding cycles considered for phase averaging is sufficient enough, a shedding cycle independency test is performed with two different numbers of shedding cycles, namely, 40 and 50 cycles. It is found that phase-averaging done with 40 and 50 shedding cycles, respectively, produces almost the same results, and hence, a shedding cycle of 50 was chosen for phase-averaging. To carry out the phase averaging, the time-signal of the lift force (C_l) acting on the stack external surface is considered as the reference signal. It has been found that the shedding frequency associated with the jet wake and stack wake, for the EJICF, remains the same and

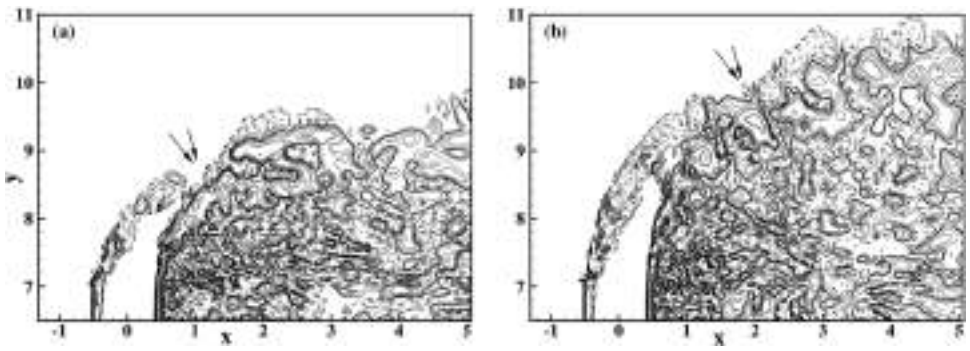

FIG. 9. Instantaneous contour of transverse-vorticity (ω_z) component showing the jet shear layer vortices on the symmetry plane $z/d = 0$ for (a) $VR = 1.5$ and (b) $VR = 2.0$. The arrows indicate the gap in the jet shear layer. Dotted contour lines indicate negative values.

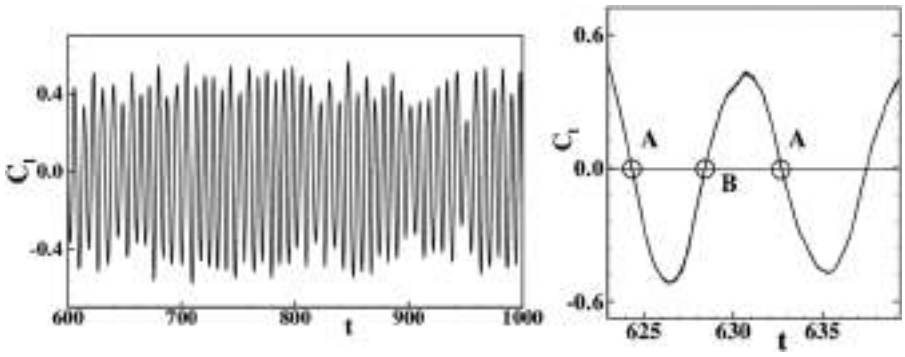

FIG. 10. Time-history of coefficient of lift (C_l) for VR = 2.0. The circled points represented by **A** and **B** represent the two opposite phases considered for phase averaging.

is discussed in detail later. The shedding frequency (Strouhal number, St) calculated using the velocity signals probed in the jet wake and stack wake gives the same dominant frequency as that calculated from the time-signal of lift force. Moreover, the signal of the lift coefficient is clean because it is a surface-averaged quantity. Therefore, the time-signal of C_l is chosen for calculating the phase-averaged flow field of both the stack wake and jet wake. Figure 10 shows the time series data of C_l and the two exactly opposite phases denoted by **A** and **B** at which phase-averaging are carried out. In the present study, the jet wake is identified as the zone just above the stack wake and below the bent-over jet, which is generally adopted definition in the open literature. Figure 11 shows the isosurfaces of phase-averaged vortical structures (λ_2-criterion) colored with the spanwise vorticity (ω_y) for all the four cases of velocity ratios. From Fig. 11, it is clearly visible that at lower VR, there is a strong interaction between the bent-over jet and the stack wake, and it becomes very difficult to distinguish the jet wake from the stack wake. However, with an increase in VR, the effective length of the stack increases and the jet wake becomes distinguishable [see Fig. 11(d)].

As discussed earlier, the low amplitude fluctuation during the symmetric mode of shedding is random lasting for a short duration, and the phase-average flow field carried out at the two chosen phases is expected to be antisymmetric. From Fig. 11(d), one can infer that similar to a stack wake, the jet wake also shows an antisymmetric mode of shedding. Similar antisymmetric modes of shedding were also reported by Kelso *et al.*[21] and Fric and Roshko[20] for the jet wake of a JICF. These vortices in the jet wake of an JICF are often referred to as upright vortices in open literature. For a JICF, it has been long debated that whether the jet can shed some of its vortices or not. While Moussa *et al.*[6] and Smith *et al.*[60] advocated that the jet can shed some of its vortices, Fric and Roshko[20] and Kelso *et al.*[21] argued that the jet cannot shed any of its vortices (no jet vortices are seen in the jet wake) and the vortices seen in the jet wake of an JICF have their origin in the wall boundary layer. However, the possibility of the existence of both jet vortices and wall vortices in the jet wake of a JICF has never been explored. The present study for an EJICF explores the possibility of the existence of both jet vortices and stack wake vortices in the jet wake. Similar to the JICF, where the wall boundary layer vortices are pulled into the jet wake to form the jet wake vortices,[20,21] in the case of EJICF, stack wake vortices are pulled into the jet wake to form the jet wake vortices due to the low pressure associated with the bent over jet. Figure 11(d) shows the formation of jet wake vortices, where the regions circled with the black line represent the jet wake vortices. These jet wake vortices are seem to

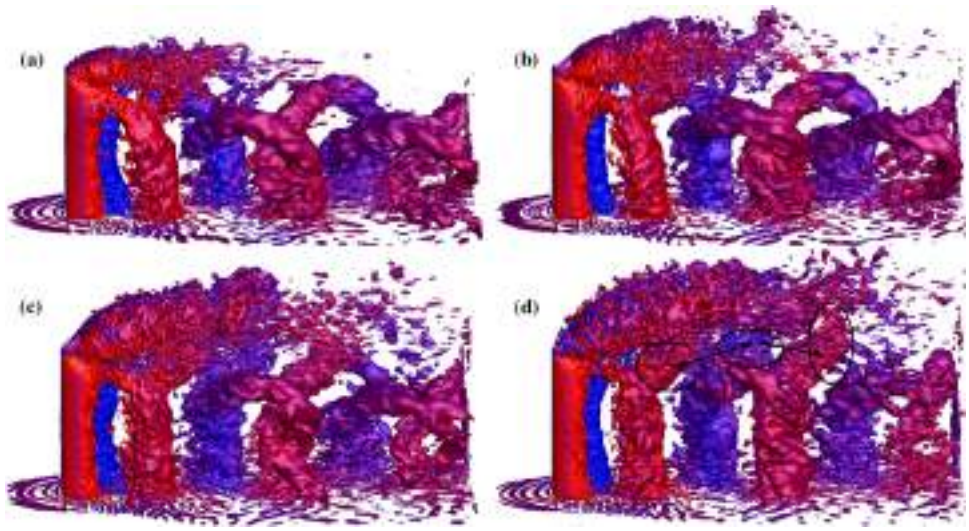

FIG. 11. Isosurfaces of phase-averaged vortical structures for velocity ratios: (a) VR = 0.5, (b) VR = 1.0, (c) VR = 1.5, and (d) VR = 2.0. The circled portion in VR = 2.0 highlights the jet wake structures.

be formed from the stack wake vortices and have their origin in the separating shear layer of the outer stack surfaces. The present study also reveals that, for an EJICF, the jet coming out of the stack itself loses some of its vortices to the jet wake, as suggested by Moussa *et al.*[6] and Smith *et al.*[60] Fric and Roshko[20] pointed out that vorticity cannot be generated at the interface of two homogeneous fluids with the same density but must be generated at the interface of a solid and fluid. Thus, for an EJICF, the jet vortices must have their origin in the boundary layer at the inner walls of the stack.

To reconfirm that the jet wake contains vortices from both the stack wake and the jet itself, the phase averaged contours of spanwise vorticity (ω_y) at various spanwise planes (x-z planes) are plotted in Fig. 12. The spanwise vorticity contours shown in Fig. 12(a) in the stack wake region, i.e., at $y = 3.5d$, reveal a close resemblance to the wake behind an infinite cylinder as expected. However, as one moves close to the stack exit, the flow field shows a shedding pattern that largely remains antisymmetric in nature but without any evidence of the shedding pattern generally observed behind an infinite cylinder. The vorticity contours in Fig. 12(b) show the distribution on one such plane close to the stack exit, $y = 6.5d$, where the wake width is found to have narrowed down significantly compared to the stack wake presented in Fig. 12(a). On the stack exit plane, $y = 7.0d$, shown in Fig. 12(c), the jet shear layer and the stack shear layer are found to coexist in the near wake, where the wake is expected to draw its vortices from the jet shear layer. On the jet wake plane, shown in Fig. 12(d), one would expect the presence of only jet shear layer vortices in the near wake, but the presence of another pair of shear layer similar to that seen on the planes, $y = 6.5d$ and 7.0, is also observed. The authors believe that these shear layers are different from those of the jet shear layer and arise because the bent-over jet pulls the vortices from the stack wake to form the jet wake. Therefore, these shear layers are referred to as trails of the stack wake shear layer in the present context. These findings also reconfirm our earlier claims that the jet wake draws its vortices from both the stack wake and the jet itself. As we move away from the jet wake to the bent-over jet region, the trails of the stack shear layer vortices vanish in the near wake, and in the bent-over jet region, i.e., vertical plane $y = 8.6d$, only jet vortices associated with the bent-over jet are observed [refer to Fig. 12(f)].

Although the stack wake vortices and jet vortices are found to coexist in the jet wake, the stack wake influences the shedding frequency associated with the jet wake. Through the experimental works, Eiff *et al.*[36] showed that there is an one-to-one lock-in between the vortices from the jet wake and stack wake. They also

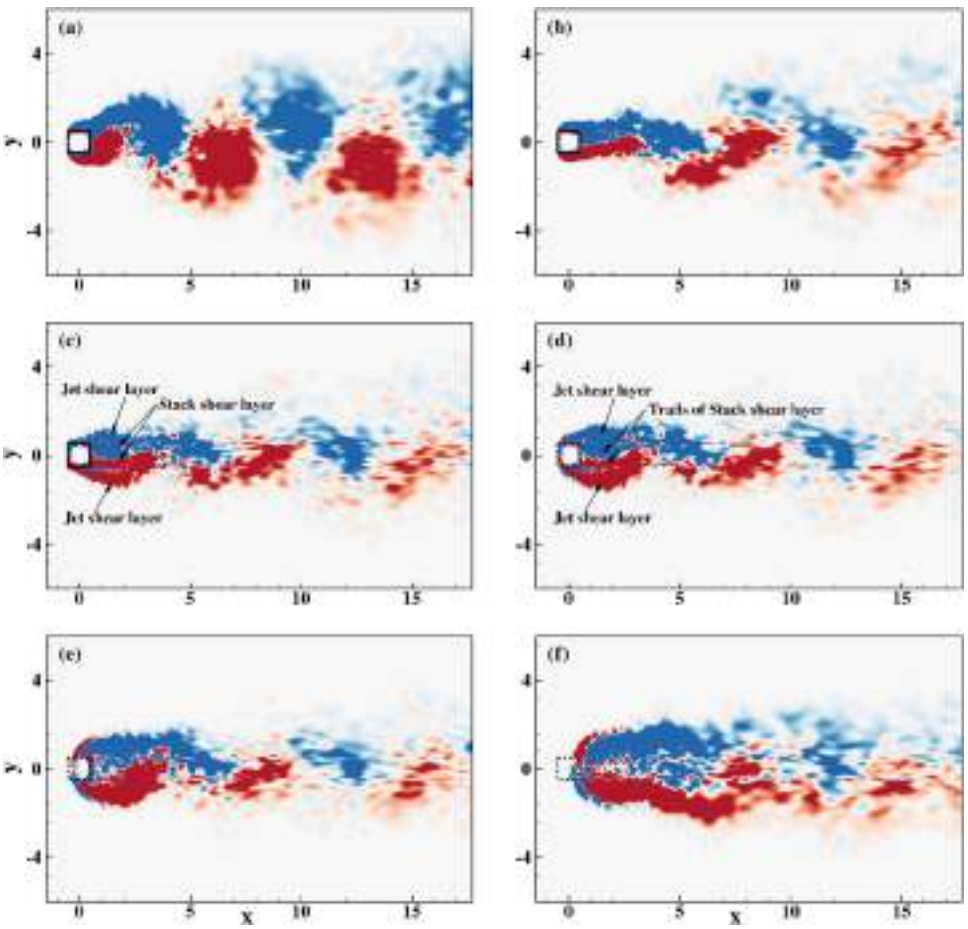

FIG. 12. Phase-averaged contours of the spanwise vorticity (ω_y) on the horizontal planes (a) $y/d = 3.5$, (b) $y/d = 6.5$, (c) $y/d = 7.0$, (d) $y/d = 7.2$, and (e) $y/d = 7.6$, and (f) $y/d = 8.6$ for velocity ratio $VR = 2.0$.

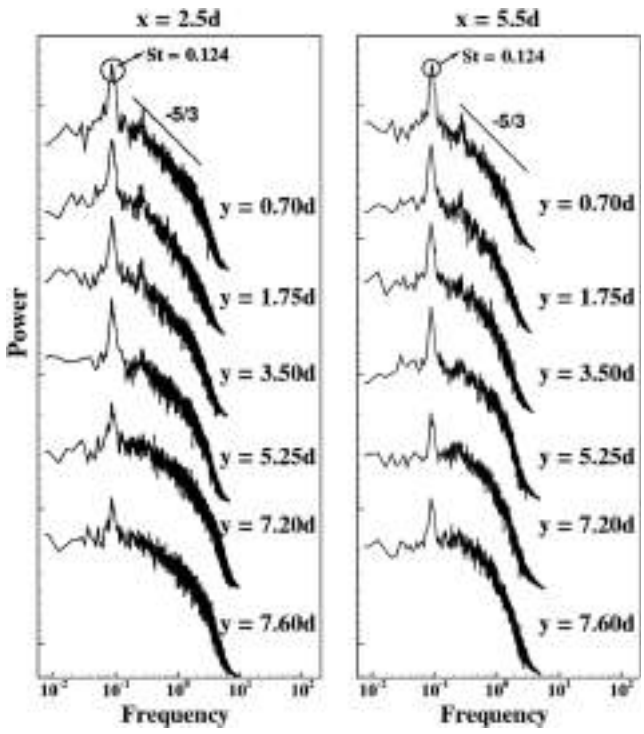

FIG. 13. Variation of the Strouhal number along the vertical axis on the symmetry plane (z/d = 0) at streamwise locations (a) x/d = 2.5 and (b) x/d = 5.5 for velocity ratio VR = 2.0.

advocated that the jet diameter has a little effect on the frequency centered activity in the jet wake and it is the stack wake that controls the frequency centered activity. The present study also agrees with the findings of Eiff *et al.*,[36] where both the stack wake and jet wake, for VR = 2.0, are observed to shed with the same dominant frequency, where the associated nondimensional frequency or Strouhal number, St, is found to be 0.124. It is also observed that the Strouhal number associated with the flow of an EJICF remains the same throughout the stack wake and jet wake. The power spectra related to the flow field behind an EJICF, across the stack wake and jet wake, for VR = 2.0, are shown in Fig. 13. The power spectra plot clearly shows that the Strouhal number (St) remains constant across the stack wake as well as the jet wake. The fixed frequency or Strouhal number, along the height of the square shaped stack, is found to be similar to the earlier findings for a wall mounted finite size square cylinder, where a fixed frequency is observed across the height of the cylinder through the presence of the jet wake. The one-to-one lock in between the stack wake and jet wake can also be noted from the phase averaged spanwise vorticity plots on the planes, y = 6.5d, 7.0d, and 7.2d, and shown in Figs. 12(b)–12(d) where the opposite signed shear layers are found to be in phase and extend almost equal distance in the streamwise direction.

The phase-averaged stream-traces are plotted in Fig. 14 in two opposite phases for VR = 2.0. From two views of the figures at two different phases, it is obvious that as expected, the phase-averaged field reveals the coherent motion of the flow. The undulation of the wake called Kármán is quite distinct in the downstream of the stack. Similarly, the formation of large scale vortices, which eventually becomes CRVP, created due to the interaction of the jet and crossflow is visible near the jet exit region. A close examination of the region near the tip of the stack shows that the shedding of the jet wake is weaker compared to the counterpart of the stack wake. At the same time, the downward movement of the stream-traces provides the evidence of the downwash flow in the stack wake region.

Based on the above analyses, the typical phase-averaged flow structure model associated with the EJICF is shown in Fig. 15. The horseshoe vortex, bent-over jet, CRVP, jet wake vortices, and stack wake vortices and their location and interaction are detailed in the sketch. The stack wake structures that shed from the opposite sides

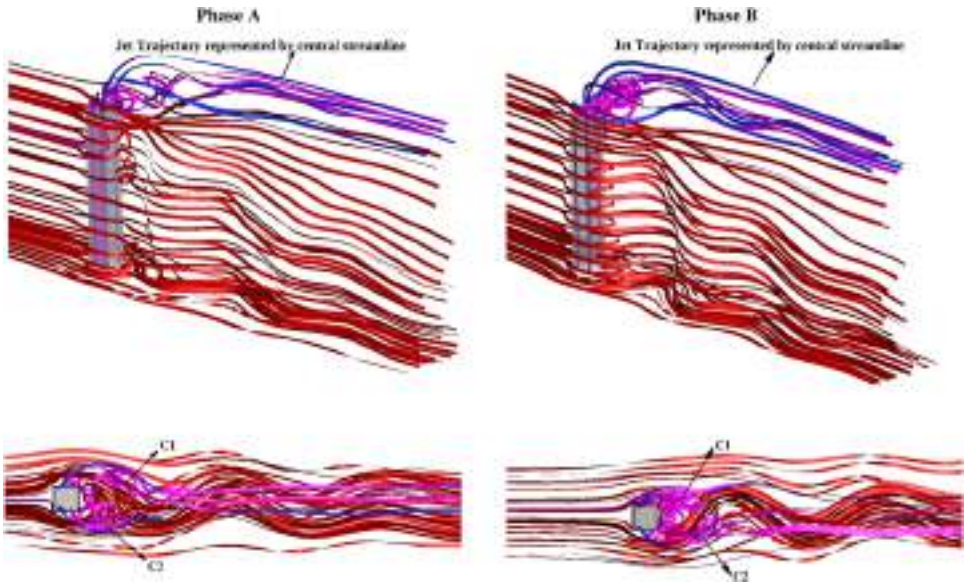

FIG. 14. Phase-averaged three-dimensional stream-traces at two exactly opposite phases, **Phase A** and **Phase B**, respectively, for VR = 2.0.

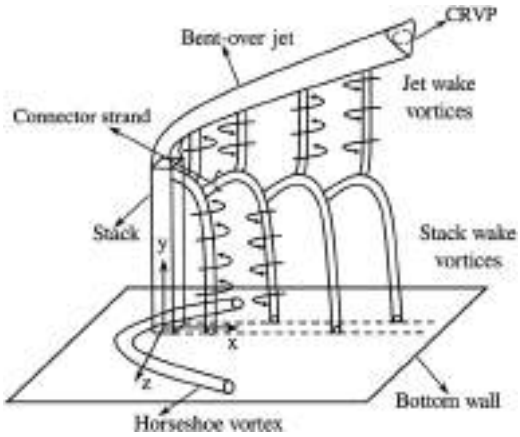

FIG. 15. Model of the flow structure around an elevated-jet in crossflow (EJICF).

of the stack are connected to each other through a connector strand similar to that observed in a wall-mounted finite-size cylinder.[61] It should be highlighted here that to satisfy the solenoidal condition of vorticity vectors, the vortex lines cannot end in a flow and should end at a wall or free-surface or must be interconnected. Therefore, similar to the stack wake structures, the jet wake structures that shed alternatively must also be interconnected in some manner in the bent-over jet region. The details of this interconnection between the alternatively shedding jet wake structures are beyond the scope of the present work. Thus, the present flow model proposed here is an approximation of the actual phase-averaged model. Although various flow structures are shown in the sketch, our emphasis is on the jet wake vortices and stack wake vortices. In particular, the relation between the jet wake and stack wake is clearly established, which was not described in the open literature for an EJICF.

D. Flow statistics

Figure 16 shows the time-averaged streamlines on the plane of symmetry $z/d = 0$. The time-averaging of data was done over a period of 1000 nondimensional time units, which are found to be independent of the averaging time. The streamline plots on the plane of symmetry, depending on the value of VR, reveal three major types of flow pattern in the wake region of an EJICF, namely, "*downwash dominated flow*," "*cross-wind dominated flow*," and "*jet dominated flow*." Figure 16(a) shows the downwash dominated flow at $VR = 0.5$, where the jet coming out of the stack does not possess enough momentum to sustain the impingement by the crossflow and hence is deflected toward the downstream wake region of the stack. It is also observed that the streamlines emitting from the stack form a vortex above the stack in the jet wake area, called *jet wake vortex*. The formation of this vortex is attributed to the interaction between the jet shear layer and the downwash imposed by the crossflow. Huang and Hsieh[42] also reported the presence of the jet wake vortex for $VR = 0.43$ and $Re_c = 2074$. They also showed that a bifurcation line that separates the recirculation zone (flow with negative streamwise velocity) from the forward moving flow, in the stack wake, evolves from the streamlines within the stack. However, in the present study, the bifurcation line seems to originate from a node point N' present in the stack wake. The difference in the origin of the bifurcation line in the present study and that of Huang and Hsieh[42] could be due to the difference in the Reynold number, aspect ratio, and shape of the cylinder. Near to the front inner face of the stack, just below the stack exit, a small vortex **H** is observed. This small vortex (**H**) was found to be absent for all the other cases of velocity ratio considered in the present study. At $VR = 0.5$, the vortex **H** is formed as the jet coming out of the stack is pushed back into the stack by the higher momentum crossflow near the front face of the stack. Kelso *et al.*[21] also observed a similar vortex for a JICF, at $VR = 2.3$ and $Re_c = 940$, called hovering vortex, above the jet exit plane near the upwind side of the jet shear layer. As the value of

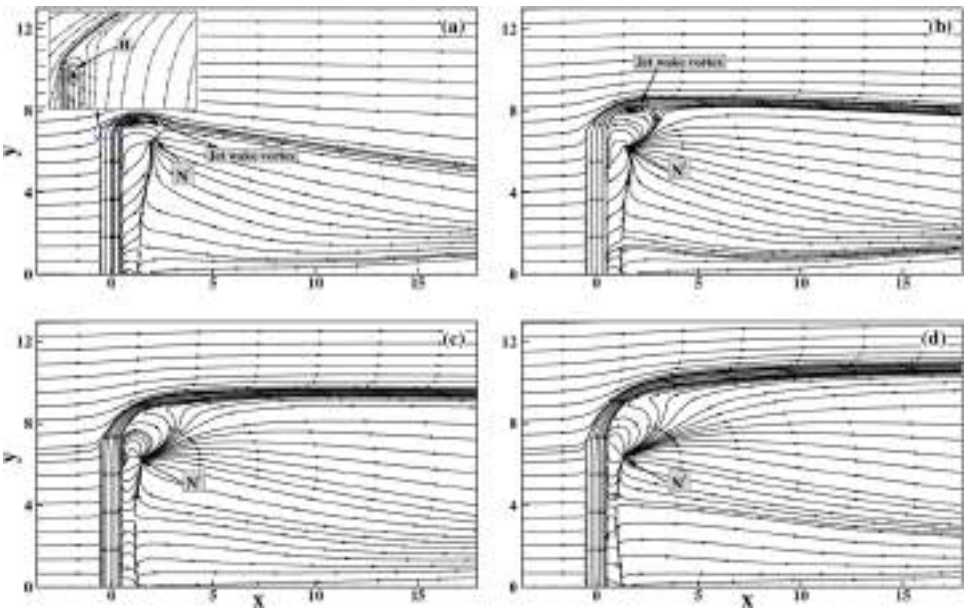

FIG. 16. Time-averaged streamlines on the symmetry plane ($z/d = 0$) for various cases of velocity ratios: (a) $VR = 0.5$, (b) $VR = 1.0$, (c) $VR = 1.5$, and (d) $VR = 2.0$.

velocity ratio is increased to $VR = 1$, the jet penetrates little more into the crossflow than that at $VR = 0.5$, thus leading to shifting of the jet wake vortex higher in the crossflow. It is also noted that the stack wake height becomes more in the downstream because of the higher penetration of the jet compared to the case of $VR = 0.5$. The other major notable difference between the downwash dominated and crossflow dominated flow is that, in the case of downwash dominated flow ($VR = 0.5$), a few streamlines coming out of the stack or, in other words, partial flow from the stack participate in the formation of the jet wake vortex, whereas for the crossflow dominated flow ($VR = 1.0$), jet flow emanating from the stack does not contribute to the jet wake vortex phenomenon. It is found that the flow originating from the node N', present in the stack wake, connects itself to the jet wake vortex, suggesting the jet vortex being fed partially by the node for its sustenance. For $VR > 1$, the flow is addressed as jet dominated flow and the jet originating from the stack is found to have enough momentum to sustain the impact of the crossflow leading to its smaller deflection toward the downstream direction. As the jet moves up in the vertical direction after its exit from the stack, it gradually loses its momentum to the crossflow and bends significantly in the streamwise direction beyond a vertical distance of $y/d > 9$. Unlike the downwash dominated flow and crosswind dominated flow, no evidence of any jet wake vortex and the associated saddle point is observed in the case of the jet dominated flow. This may be probably due to the strong shear associated with the jet that may have stretched away the jet wake vortex and the associated saddle point. Also, viscous diffusion, which is effective at small scales, is responsible for their disappearance. However, the node N' exists between the stack wake and jet wake with only difference being its relative position. It is also observed that the bifurcation line, separating the recirculation zone and forward flow, comes closer to the rear face of the stack with increasing VR. Huang and Hsieh[42] reported the flow topology on the symmetry plane for $VR = 2.02$ and advocated that it falls in a transitional regime, where a stack wake recirculation bubble is also present. They also highlighted that in the regime, $1.90 \pm 0.03 < VR < 5.90 \pm 0.10$, the flow topology of the symmetry plane varies, and they categorized it as different types of flow such as type 1, type 2, type 3, and type 4. However, the present study at $VR = 2.0$ does not show any kind of stack wake recirculation bubble in the wake region of the stack. It is also observed that the symmetry plane topology in the present study for the jet dominated flow ($VR = 1.5$ and 2.0) has close similarity to the jet dominated flow ($VR = 9.37$ and 17.36) topology of Huang and Hsieh.[42] The difference in the value of VR for the jet dominated flow regime in the present study and that of Huang and Hsieh[42] may be attributed to three major factors, i.e., the Reynolds number, the aspect ratio (AR) of the cylinder, and the stack cross-sectional shape. While the present study uses a stack with square cross section and aspect ratio $AR = 7$,

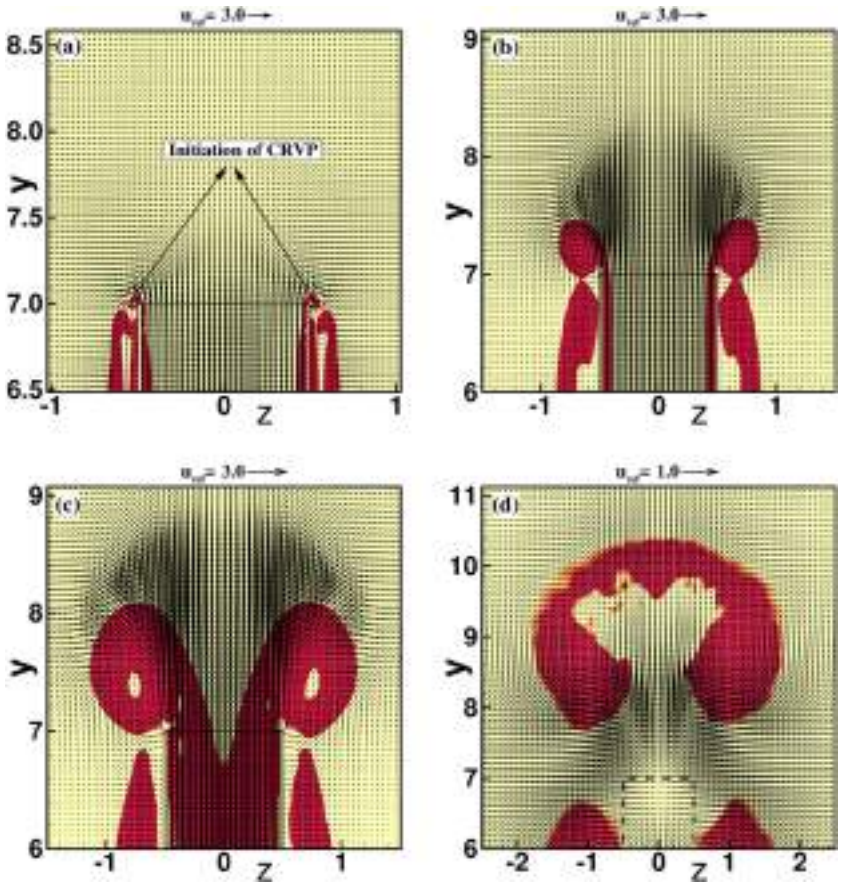

FIG. 17. Time-averaged vectors and contours of λ_2 criterion showing the streamwise evolution of CRVP on various streamwise planes: (a) $x/d = -0.4$, (b) $x/d = 0.0$, (c) $x/d = 0.4$, and (d) $x/d = 4.0$.

Huang and Hsieh[42] used a circular tube with the aspect ratio as large as $AR \approx 16$.

In order to investigate the spatial evolution of counter-rotating-vortex-pair (CRVP), the time-averaged velocity vectors and contours of λ_2, for $VR = 2$, are plotted in Fig. 17 at various planes normal to the streamwise direction. The formation of CRVP in the case of an EJICF is found to be similar to that of a JICF, where the roll-up of the lateral jet shear layer emanating out of the stack indicates the beginning of the inception of CRVP. Figure 17(a) shows the initiation of CRVP on the plane $x/d = -0.4$, where the vector plot reveals a mushroomlike flow structure with lateral folding of the jet shear layer (more clearly represented by the contours of λ_2) coming out of the pipe. The subsequent plots in Fig. 17 reveal the gradual evolution of the CRVP in the downstream direction of the jet. These findings from the present study are found to be consistent with the experimental findings of Haven and Kurosaka[62] and numerical studies of Sau *et al.*[63] for a JICF. The process of evolution of CRVP for all other cases of VR is also found to be similar to that of $VR = 2$ and is not shown here. Although the process of evolution of CRVP is found to be similar at all the values of VR considered in the present study, but the overall strength of the CRVP is found to increase with increasing VR.

The time-averaged stream-traces capturing the important flow features associated with the EJICF are presented in Fig. 18, where the different stream-traces have different sources of origin for $VR = 2.0$. The plot reveals rapid spiraling of stream-traces near both the sidewalls of the stack, stack wake region, jet wake region, and in the region of CRVP. The green stream-traces in Fig. 18 reveal the presence of a pair of symmetrically placed recirculation bubbles on either side of the stack outer walls with opposite sense of rotation. These symmetrically placed recirculation bubbles are formed due to the separation of flow at the leading edges of the square stack and their subsequent reattachment to the cylinder walls. The blue, red, and pink spiraling stream-traces along the stack height represent the stack wake recirculation region. The blue stream-traces also reveal that in the near wake of the stack wake, within the recirculation zone of the stack, the wall vortices developed on the bottom-wall are also seen to be drawn into the wake of the stack. The top view of the stream-traces plot reveals that a group of stream-traces (pink) spirals rapidly to represent the counter-rotating-vortex-pair, C1 and C2. It is already discussed that the lateral jet shear layer coming out of the stack rolls up near the jet exit to initiate the formation of CRVP. The stream-traces plotted here show that as the CRVP develops, it entrains fluid from the stack wake and grows in size as it moves downstream. The two vortices that form the time-averaged CRVP are found to be symmetric. However, the phase-averaged flow field reveals the CRVP to be asymmetric. This also confirms that the CRVP is strongly influenced by the stack wake in the case of an EJICF.

The topology of the flow field on the various horizontal planes across the span of the stack is presented through two-dimensional streamlines drawn using in-plane velocity components in Fig. 19 for $VR = 2.0$. The size of the recirculation region adjacent to the two transverse sides in the stack wake remains almost constant across

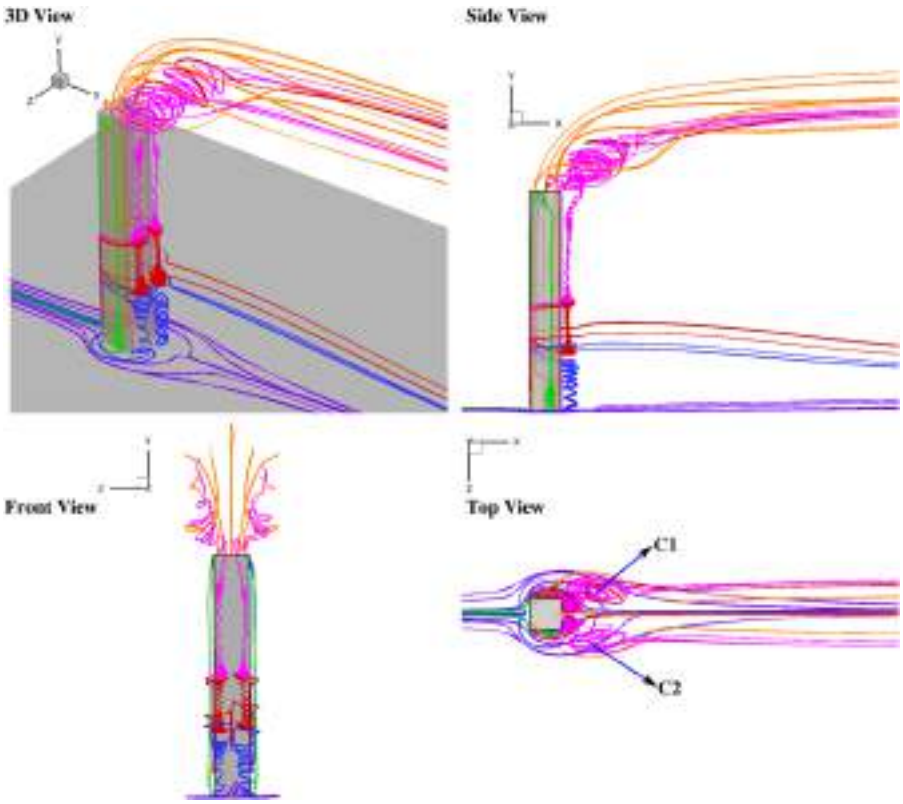

FIG. 18. Time-averaged stream-traces for $VR = 2.0$.

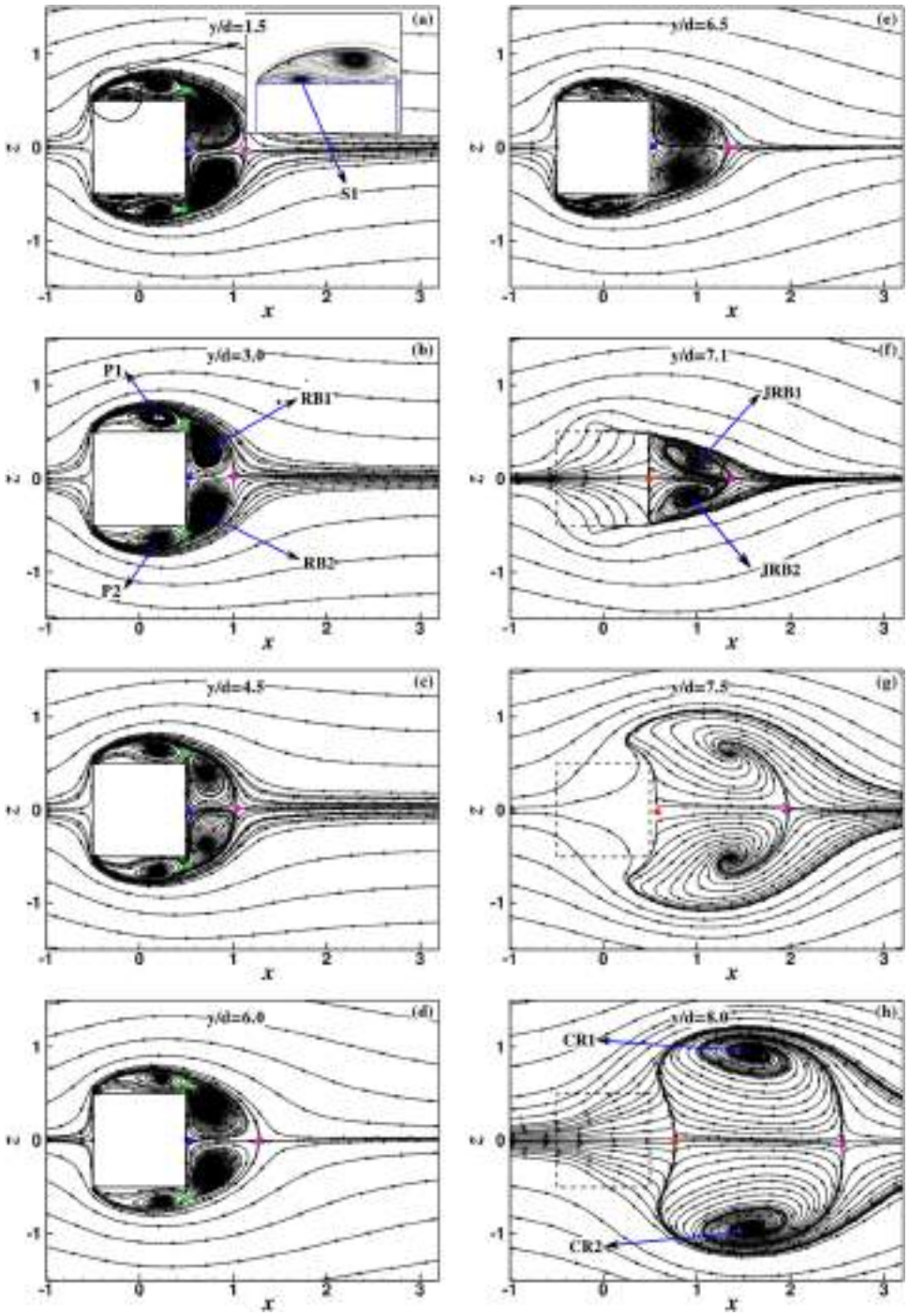

FIG. 19. Time-averaged streamlines on various horizontal planes for $VR = 2.0$.

the stack height or span except close to the free-end of the stack [Figs. 19(a)–19(d)]. However, the recirculation bubbles at the rear side of the stack vary though not significantly along the span of the stack, which is also quite obvious from streamlines on the mid-transverse plane shown in Fig. 16. As we move close to the jet exit plane [Figs. 19(e) and 19(f)], the symmetrically placed recirculation bubbles are found to get elongated in the streamwise direction with a decrease in its width. Therefore, the size of the recirculation length in the wake region close to the stack exit plane, $y/d = 6.5$ and $y/d = 7.1$, is found to be higher than that of the stack

wake. As discussed earlier, the CRVP entrains fluid from the stack wake through the jet wake as it develops spatially in the flow direction. Therefore, to satisfy the law of mass conservation, a strong entrainment of free-stream fluid from all the sides to the wake region close to the jet exit plane region is observed. As a result, the recirculation bubbles in the region close to the jet exit plane get elongated in the streamwise direction while their overall width decreases in size. In Figs. 19(a)–19(e), the symmetrically placed recirculation bubbles with opposite sense of rotation are called stack wake recirculation bubbles represented as **RB1** and **RB2**, respectively. The jet wake recirculation bubbles on the plane $y/d = 7.1$ and shown in Fig. 19(f) are represented as **JRB1** and **JRB2**, respectively. The recirculation bubbles, **CR1** and **CR2**, shown in Figs. 19(g) and 19(h) actually represent the CRVP. As discussed earlier, recirculation regions are also observed on the sides of the stack wall due to flow separation at the leading edge of the stack, which is found to be absent in the region of the jet exit plane, $y/d > 7.0$. Therefore, it suggests that the formation of the jet wake vortices is fundamentally different from that of the flow past solid obstacles, and thus, the earlier analogies[32] that the vortex shedding in the jet wake is similar to that of solid obstacles may not be true. Apart from this primary recirculation regions, represented as **P1** and **P2**, respectively, secondary recirculation regions having an opposite sense of rotation to that of the primary recirculation regions are also found to be present adjacent to the transverse walls of the stack along the stack height or span. This secondary recirculation region, **S1**, on one to the planes, $y/d = 1.5$, is shown in Fig. 19(a). The sidewall recirculation bubbles and the wake recirculation bubbles along the stack height are found to be separated by the presence of a saddle point, which is represented by the green bullets in Figs. 19(a)–19(d). Apart from that, the forward accelerating flow and the recirculation regions in the wake region are found to be separated by the saddle point represented by the pink bullets in Figs. 19(a)–19(h). Along the height of the stack, half saddle points are also observed, which are represented by the blue bullets in Figs. 19(a)–19(e).

The time-averaged three-dimensional vortex structures captured using λ_2 criterion for different velocity ratios are shown in Fig. 20. The vortex structures for all cases of velocity ratios clearly reveal the formation of a pair of streamwise vortex structures having opposite sense of rotation near the tip region of the stack. These tip vortex structures are associated with the connector strand that connects the stack wake structures that shed from either side of the stack surfaces (refer to Fig. 15). In case of higher velocity ratios ($VR \geq 1$), another pair of streamwise vortex structures having opposite sense of rotation is also observed in the jet wake region of the EJICF. These streamwise structures are associated with the evolution of the CRVP. The evolution and strength of these two pairs of streamwise structures and their dependency on the velocity ratios on the streamwise planes are also shown through the vector plots in Fig. 21.

The time-averaged velocity vector on a cross-stream location $x/d = 6$ has been shown in Fig. 21. The vector field for $VR = 0.5$ reveals the presence of a strong downwash flow in the stack wake region. The presence of a counter-rotating vortex pair just below the tip region of the stack, along with the presence of strong downwash flow, will be addressed as tip-vortices hereafter. Similar to $VR = 0.5$, the other cases of VR also show the evidence of tip-vortices. However, the strength of the tip-vortices is found to decrease with an increase in VR. The decrease in the strength of tip-vortices is associated with the weakening of the downwash flow near the tip region of the stack with increasing VR. At the plane $x/d = 6$, no CRVP has been seen in the zone above the stack wake for $VR = 0.5$, while a weaker CRVP can be noted for $VR = 1.0$. However, at higher values of VR, i.e., $VR > 1.0$, the presence of stronger CRVP, far away from the plane of inception, is quite obvious. The absence of CRVP at $VR = 0.5$ and its presence at higher VR are associated with the higher vertical penetration and strength of the jet as the strength of

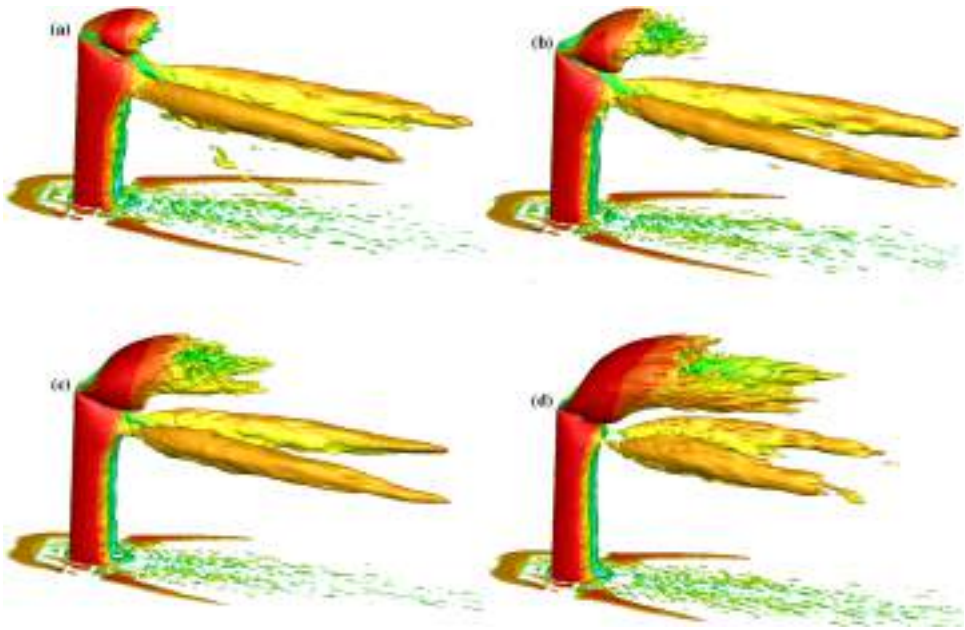

FIG. 20. Isosurfaces of time-averaged $\lambda_2 = -0.02$ showing the streamwise vortex structures for various velocity ratios: (a) $VR = 0.5$, (b) $VR = 1.0$, (c) $VR = 1.5$, and (d) $VR = 2.0$.

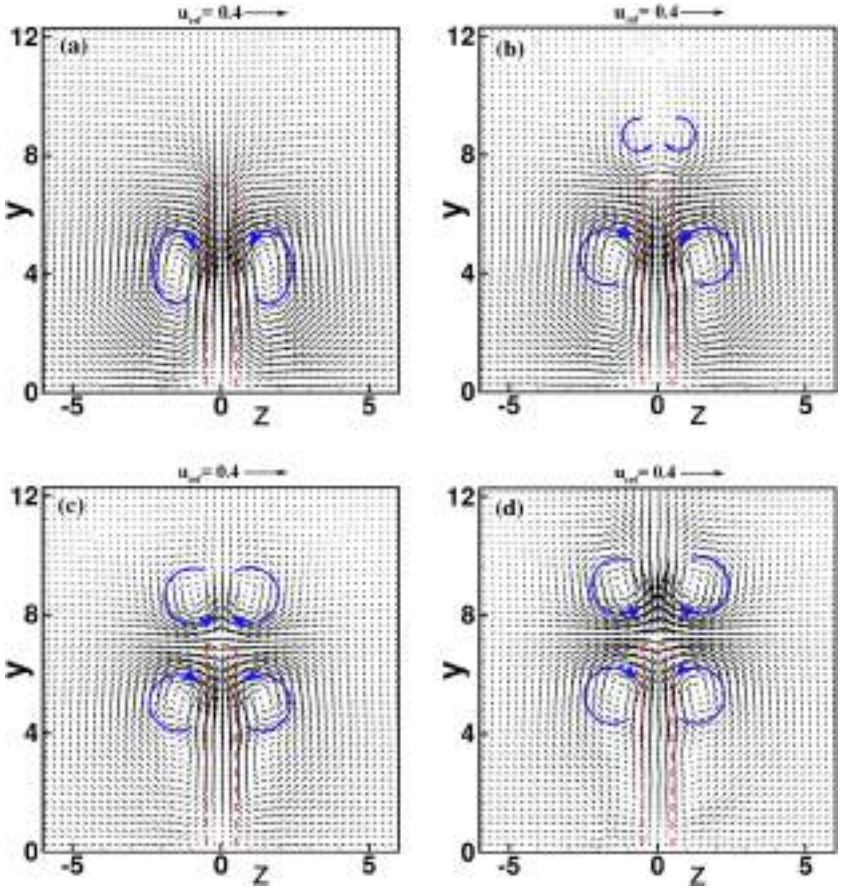

FIG. 21. Time-averaged vectors on the plane $x/d = 6.0$ for various velocity ratios: (a) $VR = 0.5$, (b) $VR = 1.0$, (c) $VR = 1.5$, and (d) $VR = 2.0$.

the jet is found to increase with an increase in VR. These findings in the far field plane at $x/d = 6$ are found to be consistent with the experimental findings of Adaramola *et al.*,[44] where experiments on a circular stack of $AR = 9$ has been conducted at $Re = 2.3 \times 10^4$. Apart from the CRVP (at higher VR) and tip-vortices, they also highlighted the presence of another pair of counter-rotating vortices near the bottom-wall, referred to as base vortices in open literature. The presence of base vortices in their study is associated with the thicker bottom-wall boundary layer thickness considered in their study, where the ratio of the bottom-wall boundary layer thickness (δ) to the height of stack (h) is given as $\delta/h = 0.5$. Since the ratio of δ/h is very small in the present study ($\delta/h \approx 0.014$), the base vortices were found to be absent for all the cases of VR considered in the present study.

Figure 22(a) presents the mean vertical velocity ($\overline{v}$) profile on the plane of symmetry, $z = 0$, across the streamwise width of the stack at various vertical locations, namely, $y = 6.0$, 7.0, 7.7, and 8.4, for $VR = 2.0$. The other VR cases are not shown as they vary only in magnitude but show a trend similar to that of $VR = 2.0$. It is clearly observed that the flow decelerates and bends toward the right side, as it comes out of the stack and interacts with the crossflow. As a result, the peak value of the vertical velocity profile decreases and shifts toward the right for planes vertically away from the stack exit.

The profiles of the normal stress ($\overline{v'v'}$) across the width of the stack, i.e., $x = -0.5$ to $x = 0.5$, are presented in Fig. 22(b). Similar to the profiles of $\overline{v}$, the peaks of the profile of $\overline{v'v'}$ also shift to the right as one moves away from the stack exit plane ($y = 7.0$). It is also observed that the normal stress $\overline{v'v'}$ is significantly enhanced over the width compared to its counterpart at $y = 7.0$ as the jet coming out of the stack interacts with the crossflow.

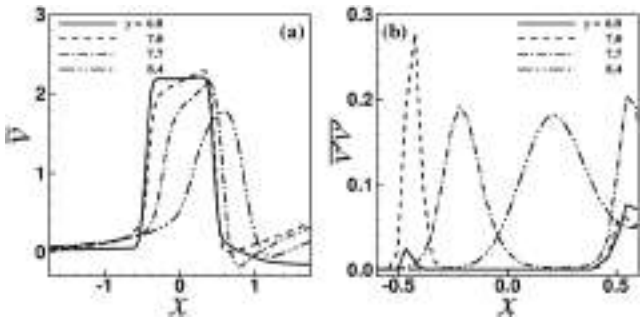

FIG. 22. Profiles of vertical velocity ($\overline{v}$) and normal stress ($\overline{v'v'}$) across the stack width on the symmetry plane $z/d = 0$ at various horizontal planes.

The flow statistics along the central streamline (called jet trajectory) on the plane $z/d = 0$, for various cases of velocity ratios (VR), are plotted in Fig. 23. The time-mean central streamlines for various velocity ratios are shown in Fig. 23(a). The jet trajectory clearly reveals the jet penetration, with $VR = 2$ having the maximum penetration and $VR = 0.5$ having the minimum penetration. To analyze the flow statistics along the jet trajectory, a new coordinate, s, is defined along the jet trajectory. The variation of various statistical quantities along this coordinate (s) is shown in Figs. 23(b)–23(d). The time-mean streamwise velocity distribution ($\overline{u}$) shown in Fig. 23(a) attains a peak value away from the stack/jet exit plane, and the peak value is found to shift constantly along the jet trajectory with the increase in VR. The shifting of the peak along the jet trajectory with VR suggests that the bending of the jet under the influence of crossflow is delayed, as the strength of the jet increases with VR. It also becomes clear from Fig. 23(a) that the peak value of the mean streamwise velocity ($\overline{u}$) along the central streamline also increases with VR. The increase in the peak value of $\overline{u}$ with VR is due to the higher momentum transfer from the jet to cross-flow at higher VR. The mean vertical velocity ($\overline{v}$) distribution along the jet trajectory, plotted in Fig. 23(c), shows a rapid decrease in $\overline{v}$ as the jet comes out of the stack and then gradually attends a constant low value in the downstream region. The gradual decrease in the $\overline{v}$ value suggests the gradual transfer of momentum from the jet fluid to the crossflow fluid, as the jet and crossflow interacts. For $VR = 0.5$, $\overline{v}$ becomes negative valued beyond the downstream region, reconfirming the earlier suggestion that, at $VR = 0.5$, the flow pattern is downwash dominated. As discussed earlier, with the increase in VR, the strength of downwash decreases and as a result $\overline{v}$ remains positive for the jet dominated

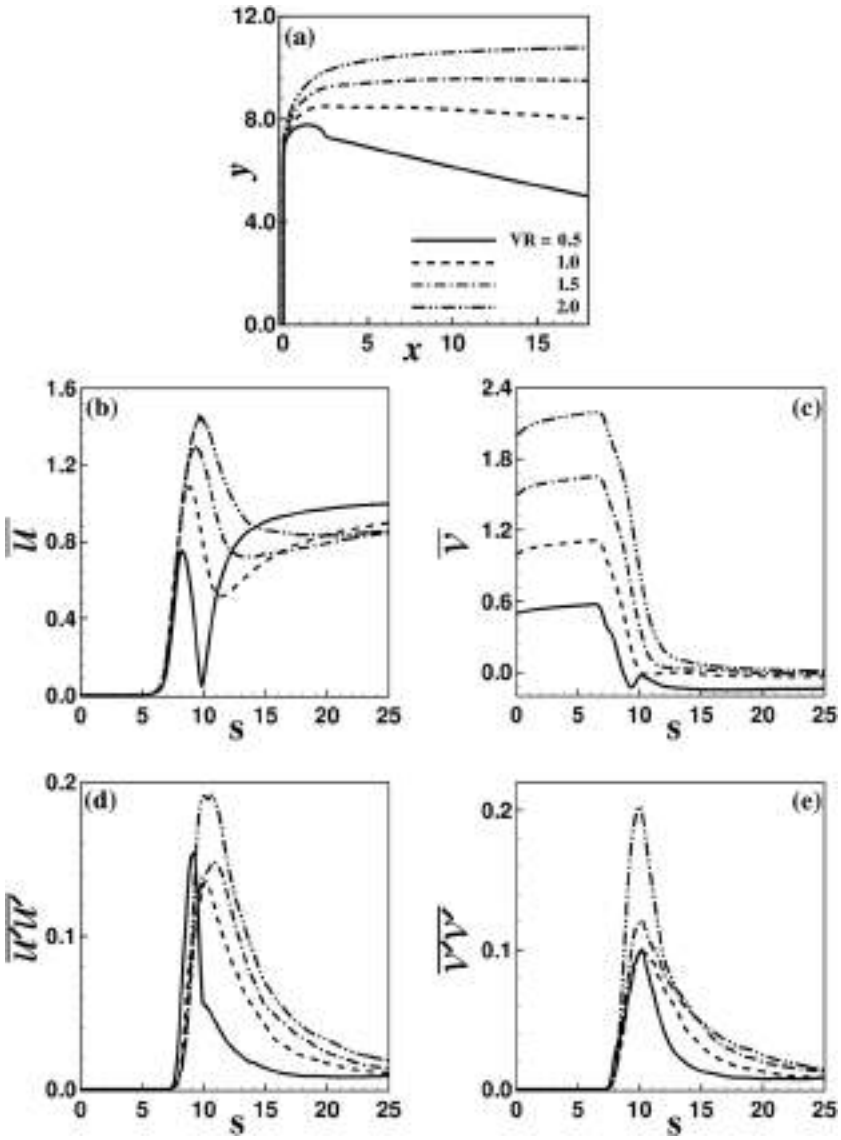

FIG. 23. Comparison of flow statistics with VR along the central streamline.

flows, i.e., for $VR > 1.0$, even in the downstream region of the flow.

The distribution of normal stresses ($\overline{u'u'}$ and $\overline{v'v'}$) associated with the central streamline is shown in Figs. 23(d) and 23(e), respectively. It is observed that both $\overline{u'u'}$ and $\overline{v'v'}$ increase quickly along the central streamline beyond the stack exit due to the impact and shear developed by the crossflow. After reaching a peak, these normal stresses decrease drastically to approach a lower value in the downstream region. The turbulence induced by the exchange of momentum between the jet and crossflow is found to be maximum for the jet dominated flows compared to the downwash dominated and crossflow dominated flows.

The time-mean jet central streamline along with the contours of the turbulent kinetic energy (TKE, $k = \overline{u_i' u_i'}$), on the plane of symmetry ($z = 0$), is shown in Fig. 24 at various VR. The embedded plots in Fig. 24 show the axial distribution of the TKE across the axial width of the stack at various vertical planes. The interaction of crossflow and the jet produces turbulence both in the stack wake and jet shear layer. Therefore, a higher level of TKE has been observed in the stack wake as well as in the shear layer of the jet. Figure 24 reveals that the downstream side of the jet shear layer, below the mean jet trajectory, has the maximum TKE content compared to the upstream side of the jet shear layer. The TKE in the trailing jet shear layer is found to increase with an increase in VR. The highest TKE region is found in the downstream of the stack where the two separating shear layers from either side of the stack are expected to interact. Moreover, the velocity shear in the near stack wake region is quite significant. The spatial extent of the high TKE region is found to increase with increasing VR. The line plot for the TKE, embedded in Fig. 24, close to the jet exit plane $y = 7.1$, reveals that the TKE near the leading and trailing edges of the jet exit plane shows a strong dependence on the VR. Comparison of the plots at various VR shows that the magnitude of TKE near the leading and trailing edges is comparable at low VR, while their relative magnitude near the two locations varies significantly at higher VR. The distribution of TKE is governed by the production of TKE, which depends on the gradients of mean velocity and the correlations of the velocity fluctuation fields. In the region above the jet exit, the mean velocity gradients $\frac{\partial \overline{u}}{\partial y}$, $\frac{\partial \overline{v}}{\partial x}$, $\frac{\partial \overline{u}}{\partial x}$, and $\frac{\partial \overline{v}}{\partial y}$ are observed to be the dominant leading to higher production of TKE. In the downstream region, a zone of lower TKE is observed between the stack wake and the downstream jet shear layer because of the reduction in the velocity shear and the velocity fluctuation.

The distribution of the TKE associated with the various axial planes, as the jet advects downstream, for $VR = 2$ is shown in Fig. 25. The contour lines of λ_2 are drawn on each plot shown in Fig. 25 to indicate the location of CRVP. At an axial location of $x = -0.4$, shown in Fig. 25(a), a maximum TKE is found to be associated with the lateral jet shear layer emerging out of the stack, which is responsible for the initiation of the CRVP formation. As the CRVP evolves, the TKE is found to be concentrated in the recirculatory region of the CRVP. The two recirculatory regions of the CRVP on either side of the centerline is seen to contain less TKE as expected. However, at the axial location of $x = 4$, the TKE associated with the CRVP is observed to be much less than that at the upstream locations because of the viscous diffusion of the CRVP as the jet advects downstream.

Figure 26 illustrates the lateral distribution of time-averaged streamwise and spanwise velocity, at the streamwise location $x/d = 2.0$, at four different spanwise planes, $y/d = 4.0$, 7.0, 7.7, and 8.4. The streamwise velocity profile at the plane $y = 4.0$ shows a decrease in velocity deficit with an increase in the magnitude of VR with maximum velocity deficit to be observed for $VR = 0.5$. The decrease in velocity deficit, in the stack wake, with an increase in VR can be due to the decrease in the strength of the downwash with increasing VR. At low VR, the jet does not possess enough momentum

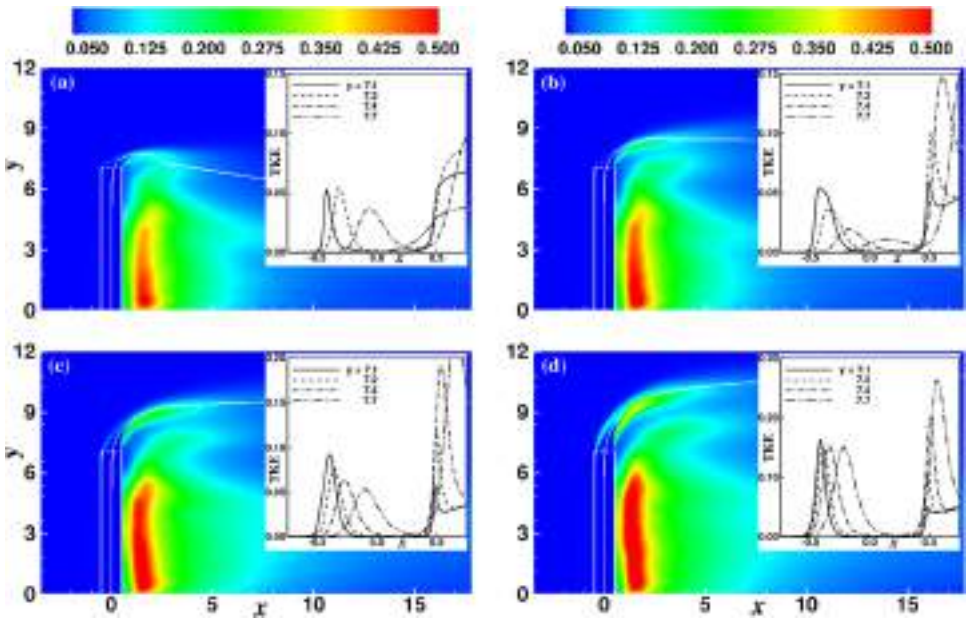

FIG. 24. Contours of turbulent kinetic energy on the symmetric plane, $z/d = 0$, for various velocity ratios: (a) $VR = 0.5$, (b) $VR = 1.0$, (c) $VR = 1.5$, and (d) $VR = 2.0$. The embedded figures show the variation of the TKE across the stack width at various vertical locations.

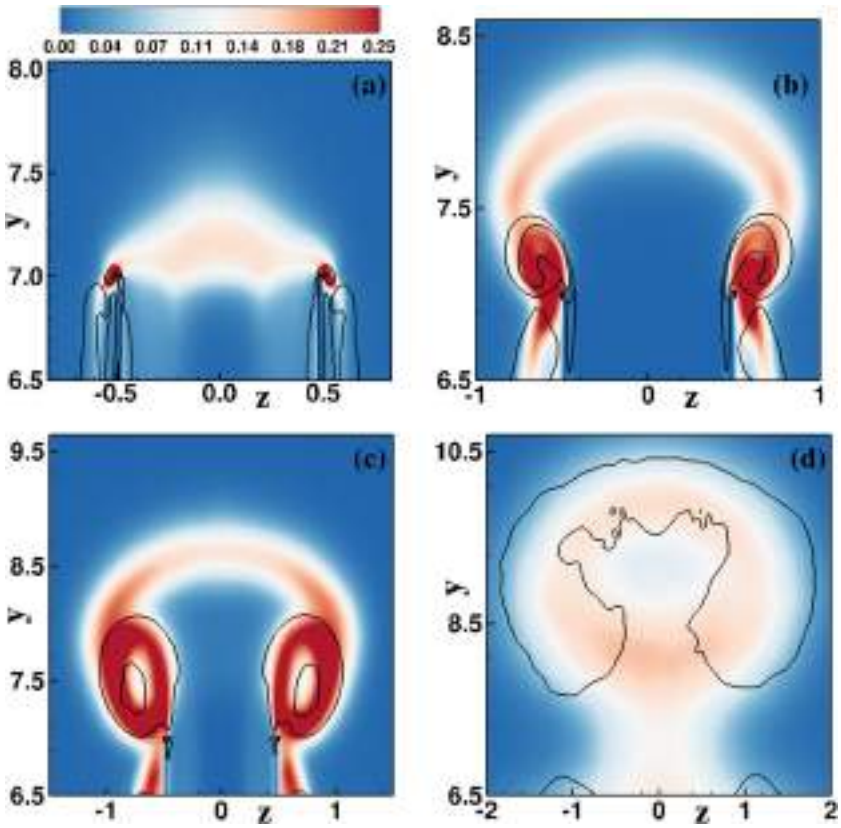

FIG. 25. Contours of turbulent kinetic energy on the streamwise planes (a) x/d = −0.4, (b) x/d = 0.0, (c) x/d = 0.4, and (d) x/d = 4.0 at velocity ratio VR = 2.0. The black contour lines of λ_2 show the position of CRVP.

to sustain the impingement of the crossflow and hence is deflected into the downstream close to the tip of the stack (see Fig. 16). As a result, the node point N' observed in the stack wake is found to be away from the stack rear face at VR = 0.5. However, the same node point is found to move closer to the stack with an increase in VR because of the fact that the jet becomes stronger with increasing VR. Therefore, the recirculation length along the stack in the case of the EJICF is found to decrease with an increase in VR (refer to

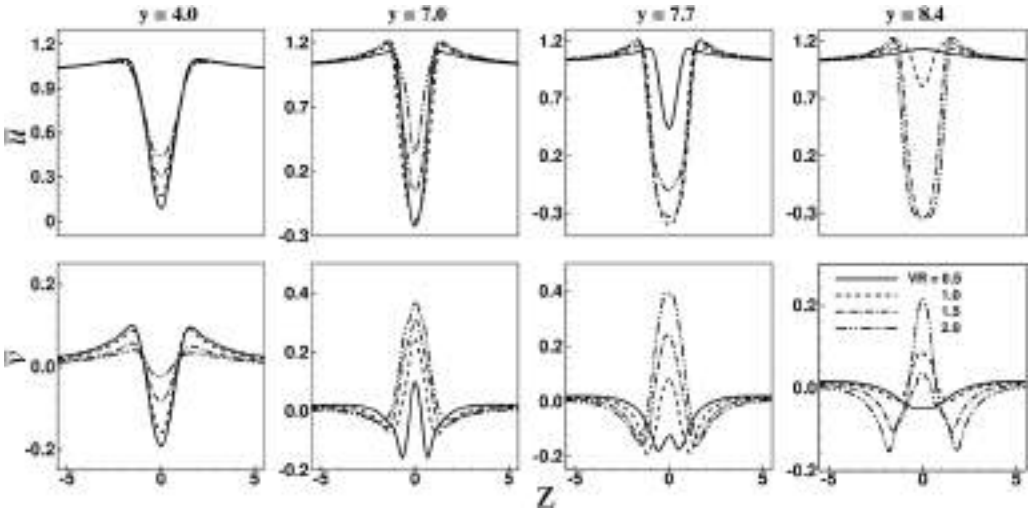

FIG. 26. Transverse variation of the time-average streamwise and spanwise velocity at the axial location, x/d = 2.0, on various horizontal planes, y/d = 4.0, 7.0, 7.7, and 8.4.

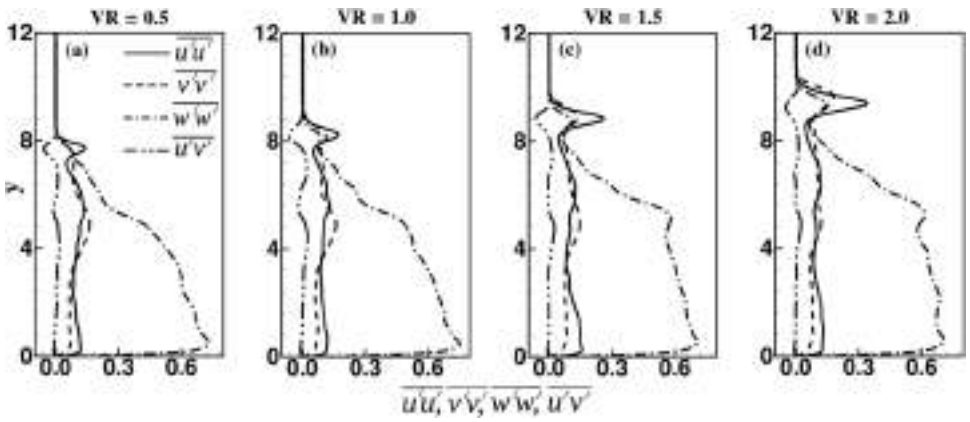

FIG. 27. Spanwise variation of normal-stresses and shear stress ($\overline{u'v'}$) on the midtransverse plane z/d = 0 at an axial location, x/d = 2.0.

Fig. 16). The streamwise velocity profile at the plane, y = 7.0, also confirms these findings, where a recirculation region (shown by the presence of negative streamwise velocity field) is found for VR = 0.5 and 1.0. However, with the increase in VR, i.e., for VR = 1.5 and 2.0, the flow field does not show the presence of any recirculation zone on the plane y = 7.0 [Fig. 26(b)]. As we move further away from the plane y = 7.0 to plane y = 7.7, the evidence of recirculation zone for VR > 0.5 has been noted, which is quite obvious from the profiles of the streamwise velocity. However, on the plane y = 8.4, only the velocity profiles associated with VR = 1.5 and 2.0 show the presence of recirculation region. The recirculation zone on the planes y = 7.7 and 8.4 at higher velocity ratios is associated with the strength of the jet penetrating deeper into the crossflow and thereby increases the effective height of the jet wake region, which is otherwise small at low VR.

The time-averaged vertical velocity profile in the stack wake plane y = 4.0 shows a stronger negative velocity field for VR = 0.5 [Fig. 26(e)], which confirms the earlier claim of the stack wake having maximum downwash for VR = 0.5. With the increase in VR, the magnitude of vertical velocity in the near wake of the stack is found to decrease, suggesting that the strength of downwash flow decreases with an increase in VR. In contrast to a wall mounted finite square cylinder [where a strong downwash flow is observed about the symmetry plane (z = 0) near the free-end plane of the cylinder], the flow near the tip plane (y = 7.0) in an EJICF shows the presence of a strong positive vertical velocity (means upwash flow) about the symmetry plane z = 0.0. The presence of the upwash flow in the case of EJICF, near the tip plane y = 7.0, is associated with the jet coming out of the stack that penetrates into the crossflow and, thus, restricts the downwash flow from the top of the stack into the wake's central zone in the near wake. The vertical velocity profile on and above the plane y = 7.0 shows a positive peak on the symmetry plane for all the cases (except for VR = 0.5 on the plane y = 8.4). The magnitude of this positive vertical velocity, which also suggests an induced upwash flow due to the CRVP, increases with an increase in VR. Apart from the positive velocity peak near the symmetry plane, the vertical velocity profile also shows two symmetrically positioned "$-v$e" velocity peaks. These "$-v$e" velocity peaks are associated with the presence of the CRVP in the jet wake. The absence of the "$+v$e" and the two symmetrically positioned "$-v$e" peaks for VR = 0.5 [Fig. 26(h)] is due to the absence of the CRVP at the plane, y = 8.4. The vertical velocity profile in Figs. 26(f) and 26(h) also suggests that as one moves vertically away from the tip of the stack toward the top vertical boundary, the strength of the CRVP decreases with decreasing VR. It also shows that the strength of the upwash flow induced by the CRVP also decreases as one moves away from the tip of the stack along vertical direction of the domain.

To further investigate the effect of jet velocity ratio (VR) on the turbulent flow field of the EJICF, the profiles of Reynolds normal stresses and shear stress ($\overline{u'v'}$) are analyzed. The distribution of the normal stresses and the shear stress, $\overline{u'v'}$ (other shear stress being very small), at the axial location $x = 2.0d$, on the symmetry plane $z = 0d$ is plotted in Fig. 27. From Fig. 27, it is clearly seen that in the stack wake, the Reynolds normal stress component $\overline{w'w'}$ is much higher than the other two components of the normal stress. Therefore, it can be argued that in the stack wake of an EJICF, similar to a wall mounted finite size cylinder, the normal stress component $\overline{w'w'}$ is the major contributor to the stack wake TKE. The higher magnitude of $\overline{w'w'}$ in the stack wake could be due to the strong mutual interaction among the shear layers, separating from the two sides of the stack. It is also observed that the jet velocity ratio has a minimal effect on the turbulent statistics of the stack wake, as the normal stresses and shear stress ($\overline{u'v'}$) distribution in the stack wake are very similar (both distribution and magnitude) at all VRs. However, in the jet wake, contrary to the stack wake, the normal stress component $\overline{u'u'}$ is found to be slightly higher than the other components of stresses. Therefore, it reconfirms our earlier claims that the mean velocity gradients $\frac{\partial \overline{u}}{\partial y}$, $\frac{\partial \overline{v}}{\partial x}$, $\frac{\partial \overline{u}}{\partial x}$, and $\frac{\partial \overline{v}}{\partial y}$ are the dominant processes for the production of TKE in the jet wake and the jet bent-over region. The normal stress components are found to increase with an increase in VR, showing the evidence of influence of VR on the turbulence of the jet flow.

IV. CONCLUSIONS

In the present study, a large eddy simulation has been carried out to investigate the effect of jet to crossflow velocity ratio on the characteristic flow features of an EJICF. The simulations are carried out at a Reynolds number of 20 000 for four different velocity ratios,

VR = 0.5, 1.0, 1.5, and 2.0. Similar to the wake of a wall-mounted finite-size cylinder, the stack wake of the EJICF also shows the presence of both antisymmetric and symmetric modes of shedding in the near wake, but only for VR = 0.5. At higher velocity ratios, only the presence of antisymmetric mode of shedding was found. It is also revealed that the velocity ratio has a strong effect on the source of vorticity of the jet shear layer (mainly on the upstream side of the jet shear layer). At VR = 0.5, the upstream side of the jet shear layer seems to draw its vortices from the outer surface of the stack boundary layer, while with an increase in velocity ratio, it seems to draw its vortices from the inner wall surface of the stack boundary layer. The downstream side of the jet shear layer is always found to draw its vortices from the inner wall surface of the stack. The present study also reveals that both stack wake vortices and jet vortices are found to coexist in the jet wake, but the shedding frequency associated with the jet wake is governed by the stack wake frequency. One to one lock in between the jet wake structures and stack wake structures is also observed. The time-averaged flow field revealed three different flow regimes depending on the magnitude of VR, namely, "downwash dominated" (VR = 0.5), "cross-wind dominated" (VR = 1.0), and "jet dominated" (VR = 1.5, 2.0) regimes. The "downwash dominated" flow regime showed the presence of only one pair of counter-rotating vortices near the tip region of stack. However, the "cross-wind dominated" and "jet dominated" flow regimes showed the presence of two pairs of counter-rotating vortices near the tip of the stack (one pair each above and below the tip region of the stack). The vortex pair above the tip region of the stack at $VR \geqslant 1.0$ corresponds to the CRVP. The inception of CRVP in the case of EJICF is found to be very similar to that observed in JICF, where the lateral folding of the stack shear layer near the jet exit seems to initiate the formation of CRVP. It is also revealed that the CRVP entrains fluid from the stack wake through the jet wake as it develops spatially in the crossflow direction.

ACKNOWLEDGMENTS

The authors would like to thank the High Performance Computational Facilities of the Computer Center, Indian Institute of Technology Kanpur, for providing the desired computational requirements for carrying out the simulations.

REFERENCES

[1]J. Keffer and W. Baines, "The round turbulent jet in a cross-wind," J. Fluid Mech. **15**, 481–496 (1963).
[2]Y. Kamotani and I. Greber, "Experiments on a turbulent jet in a cross flow," AIAA J. **10**, 1425–1429 (1972).
[3]S. Smith and M. Mungal, "Mixing, structure and scaling of the jet in crossflow," J. Fluid Mech. **357**, 83–122 (1998).
[4]E. F. Hasselbrink and M. Mungal, "Transverse jets and jet flames. Part 1. Scaling laws for strong transverse jets," J. Fluid Mech. **443**, 1–25 (2001).
[5]S. Muppidi and K. Mahesh, "Study of trajectories of jets in crossflow using direct numerical simulations," J. Fluid Mech. **530**, 81–100 (2005).
[6]Z. Moussa, J. W. Trischka, and S. Eskinazi, "The near field in the mixing of a round jet with a cross-stream," J. Fluid Mech. **80**, 49–80 (1977).
[7]S. Muppidi and K. Mahesh, "Direct numerical simulation of passive scalar transport in transverse jets," J. Fluid Mech. **598**, 335–360 (2008).
[8]J. W. Shan and P. E. Dimotakis, "Reynolds-number effects and anisotropy in transverse-jet mixing," J. Fluid Mech. **566**, 47–96 (2006).
[9]G. Rudinger and L. F. Moon, "Laser-Doppler measurements in a subsonic jet injected into a subsonic cross flow," J. Fluids Eng. **98**, 516–520 (1976).
[10]J. Andreopoulos and W. Rodi, "Experimental investigation of jets in a crossflow," J. Fluid Mech. **138**, 93–127 (1984).
[11]J. Andreopoulos, "On the structure of jets in a crossflow," J. Fluid Mech. **157**, 163–197 (1985).
[12]S. Sherif and R. Pletcher, "Measurements of the flow and turbulence characteristics of round jets in crossflow," J. Fluids Eng. **111**, 165–171 (1989).
[13]J. G. Santiago and J. C. Dutton, "Velocity measurements of a jet injected into a supersonic crossflow," J. Propul. Power **13**, 264–273 (1997).
[14]F. Génin and S. Menon, "Dynamics of sonic jet injection into supersonic crossflow," J. Turbul. **11**, N4 (2010).
[15]Z. Rana, B. Thornber, and D. Drikakis, "On the importance of generating accurate turbulent boundary condition for unsteady simulations," J. Turbul. **12**, N35 (2011).
[16]Z. A. Rana, B. Thornber, and D. Drikakis, "Transverse jet injection into a supersonic turbulent cross-flow," Phys. Fluids **23**, 046103 (2011).
[17]S. Kawai and S. Lele, "Large-eddy simulation of jet mixing in a supersonic turbulent crossflow," in *19th AIAA Computational Fluid Dynamics* (AIAA, 2009), p. 3795.
[18]J. Andreopoulos, "Measurements in a jet-pipe flow issuing perpendicularly into a cross stream," J. Fluids Eng. **104**, 493–499 (1982).
[19]J. Andreopoulos, "Heat transfer measurements in a heated jet-pipe flow issuing into a cold cross stream," Phys. Fluids **26**, 3201–3210 (1983).
[20]T. Fric and A. Roshko, "Vortical structure in the wake of a transverse jet," J. Fluid Mech. **279**, 1–47 (1994).
[21]R. M. Kelso, T. Lim, and A. Perry, "An experimental study of round jets in crossflow," J. Fluid Mech. **306**, 111–144 (1996).
[22]T. Lim, T. New, and S. Luo, "On the development of large-scale structures of a jet normal to a cross flow," Phys. Fluids **13**, 770–775 (2001).
[23]J. Blanchard, Y. Brunet, and A. Merlen, "Influence of a counter rotating vortex pair on the stability of a jet in a cross flow: An experimental study by flow visualizations," Exp. Fluids **26**, 63–74 (1999).
[24]L. Cortelezzi and A. R. Karagozian, "On the formation of the counter-rotating vortex pair in transverse jets," J. Fluid Mech. **446**, 347–373 (2001).
[25]L. L. Yuan, R. L. Street, and J. H. Ferziger, "Large-eddy simulations of a round jet in crossflow," J. Fluid Mech. **379**, 71–104 (1999).
[26]M. Landman and P. Saffman, "The three-dimensional instability of strained vortices in a viscous fluid," Phys. Fluids **30**, 2339–2342 (1987).
[27]A. Krothapalli, L. Lourenco, and J. Buchlin, "Separated flow upstream of a jet in a crossflow," AIAA J. **28**, 414–420 (1990).
[28]R. Kelso and A. Smits, "Horseshoe vortex systems resulting from the interaction between a laminar boundary layer and a transverse jet," Phys. Fluids **7**, 153–158 (1995).
[29]P. Mason and B. Morton, "Trailing vortices in the wakes of surface-mounted obstacles," J. Fluid Mech. **175**, 247–293 (1987).
[30]S. L. Coelho and J. Hunt, "The dynamics of the near field of strong jets in crossflows," J. Fluid Mech. **200**, 95–120 (1989).
[31]R. Sykes, W. Lewellen, and S. Parker, "On the vorticity dynamics of a turbulent jet in a crossflow," J. Fluid Mech. **168**, 393–413 (1986).
[32]H. McMahon, D. Hester, and J. Palfery, "Vortex shedding from a turbulent jet in a cross-wind," J. Fluid Mech. **48**, 73–80 (1971).
[33]J. Wu, A. Vakili, and F. Yu, "Investigation of the interacting flow of nonsymmetric jets in crossflow," AIAA J. **26**, 940–947 (1988).
[34]F. Schlegel, D. Wee, Y. M. Marzouk, and A. F. Ghoniem, "Contributions of the wall boundary layer to the formation of the counter-rotating vortex pair in transverse jets," J. Fluid Mech. **676**, 461–490 (2011).
[35]L. Su and M. Mungal, "Simultaneous measurements of scalar and velocity field evolution in turbulent crossflowing jets," J. Fluid Mech. **513**, 1–45 (2004).
[36]O. Eiff, J. Kawall, and J. Keffer, "Lock-in of vortices in the wake of an elevated round turbulent jet in a crossflow," Exp. Fluids **19**, 203–213 (1995).

[37]O. S. Eiff and J. F. Keffer, "On the structures in the near-wake region of an elevated turbulent jet in a crossflow," J. Fluid Mech. **333**, 161–195 (1997).
[38]R. F. Huang and J. Lan, "Characteristic modes and evolution processes of shear-layer vortices in an elevated transverse jet," Phys. Fluids **17**, 034103 (2005).
[39]N. M. Saïd, H. Mhiri, G. Le Palec, and P. Bournot, "Experimental and numerical analysis of pollutant dispersion from a chimney," Atmos. Environ. **39**, 1727–1738 (2005).
[40]N. M. Said, S. Habli, H. Mhiri, H. Bournot, and G. Le Palec, "Flow field measurement in a crossflowing elevated jet," J. Fluids Eng. **129**, 551–562 (2007).
[41]R. Huang and R. Hsieh, "An experimental study of elevated round jets deflected in a crosswind," Exp. Therm. Fluid Sci. **27**, 77–86 (2002).
[42]R. F. Huang and R. H. Hsieh, "Sectional flow structures in near wake of elevated jets in a crossflow," AIAA J. **41**, 1490–1499 (2003).
[43]M. Adaramola, D. Sumner, and D. Bergstrom, "Turbulent wake and vortex shedding for a stack partially immersed in a turbulent boundary layer," J. Fluids Struct. **23**, 1189–1206 (2007).
[44]M. Adaramola, D. Sumner, and D. Bergstrom, "Effect of velocity ratio on the streamwise vortex structures in the wake of a stack," J. Fluids Struct. **26**, 1–18 (2010).
[45]P. Arora and A. K. Saha, "Three-dimensional numerical study of flow and species transport in an elevated jet in crossflow," Int. J. Heat Mass Transfer **54**, 92–105 (2011).
[46]M. Lesieur, O. Métais, and P. Comte, *Large-eddy Simulations of Turbulence* (Cambridge University Press, 2005).
[47]E. Lévêque, F. Toschi, L. Shao, and J.-P. Bertoglio, "Shear-improved smagorinsky model for large-eddy simulation of wall-bounded turbulent flows," J. Fluid Mech. **570**, 491–502 (2007).
[48]T. B. Gohil, A. K. Saha, and K. Muralidhar, "Large eddy simulation of a free circular jet," J. Fluids Eng. **136**, 051205 (2014).
[49]F. H. Harlow and J. E. Welch, "Numerical study of large-amplitude free-surface motions," Phys. Fluids **9**, 842–851 (1966).
[50]Y. Srinivas, G. Biswas, A. Parihar, and R. Ranjan, "Large-eddy simulation of high Reynolds number turbulent flow past a square cylinder," J. Eng. Mech. **132**, 327–335 (2006).
[51]A. Sohankar, L. Davidson, and C. Norberg, "Large eddy simulation of flow past a square cylinder: Comparison of different subgrid scale models," J. Fluids Eng. **122**, 39–47 (2000).
[52]D. Lyn, S. Einav, W. Rodi, and J.-H. Park, "A laser-Doppler velocimetry study of ensemble-averaged characteristics of the turbulent near wake of a square cylinder," J. Fluid Mech. **304**, 285–319 (1995).
[53]E. Maskell, "A theory of the blockage effects on bluff bodies and stalled wings in a closed wind tunnel," Reports and Memoranda No. 3400, Aeronautical Research Council London, United Kingdom, 1963.
[54]I. Orlanski, "A simple boundary condition for unbounded flows," J. Comput. Phys. **21**, 251–269 (1976).
[55]H. Sakamoto and M. Arie, "Vortex shedding from a rectangular prism and a circular cylinder placed vertically in a turbulent boundary layer," J. Fluid Mech. **126**, 147–165 (1983).
[56]H. Wang, Y. Zhou, C. Chan, and K. Lam, "Effect of initial conditions on interaction between a boundary layer and a wall-mounted finite-length-cylinder wake," Phys. Fluids **18**, 065106 (2006).
[57]H. F. Wang and Y. Zhou, "The finite-length square cylinder near wake," J. Fluid Mech. **638**, 453–490 (2009).
[58]S. Behera and A. K. Saha, "Characteristics of the flow past a wall-mounted finite-length square cylinder at low Reynolds number with varying boundary layer thickness," J. Fluids Eng. **141**, 061204 (2019).
[59]J. Andreopoulos, "Wind tunnel experiments on cooling tower plumes: Part 1—In uniform crossflow," J. Heat Transfer **111**, 941–948 (1989).
[60]S. Smith, A. Lozano, M. Mungal, and R. Hanson, "Scalar mixing in the subsonic jet in crossflow," in *Computational and Experimental Assessment of Jets in Cross Flow*, No. SEE N94-28003 07-34 (AGARD, 1993), p. 13.
[61]J. Bourgeois, P. Sattari, and R. Martinuzzi, "Alternating half-loop shedding in the turbulent wake of a finite surface-mounted square cylinder with a thin boundary layer," Phys. Fluids **23**, 095101 (2011).
[62]B. Haven and M. Kurosaka, "Kidney and anti-kidney vortices in crossflow jets," J. Fluid Mech. **352**, 27–64 (1997).
[63]A. Sau, T. W. Sheu, S. Tsai, R. R. Hwang, and T. Chiang, "Structural development of vortical flows around a square jet in cross-flow," Proc. R. Soc. London, Ser. A **460**, 3339–3368 (2004).